Forschungszentrum Karlsruhe
in der Helmholtz-Gemeinschaft

Wissenschaftliche Berichte
FZKA7002

KAJET Experiments on Pressure-Driven Melt Jets and their Interaction with Concrete

G. Albrecht, F. Huber, E. Jenes, A. Kaiser, W. Schütz

Institut für Reaktorsicherheit
Programm Nukleare Sicherheitsforschung

Februar 2005

Forschungszentrum Karlsruhe

in der Helmholtz-Gemeinschaft

Wissenschaftliche Berichte

FZKA 7002

KAJET Experiments on Pressure-Driven Melt Jets and their Interaction with Concrete

G. Albrecht, F. Huber, E. Jenes, A. Kaiser, W. Schütz

Institut für Reaktorsicherheit

Programm Nukleare Sicherheitsforschung

Forschungszentrum Karlsruhe GmbH, Karlsruhe

2005

Impressum der Print-Ausgabe:

Als Manuskript gedruckt
Für diesen Bericht behalten wir uns alle Rechte vor

Forschungszentrum Karlsruhe GmbH
Postfach 3640, 76021 Karlsruhe

Mitglied der Hermann von Helmholtz-Gemeinschaft
Deutscher Forschungszentren (HGF)

ISSN 0947-8620

urn:nbn:de:0005-070027

Abstract

In case of a localized RPV failure, the melt expulsion into the reactor cavity may be as a compact jet for a short period, following by a dispersed release after gas break-through. The KAJET experiments were related to the short initial phase of a compact jet. The main objective of the experiments was to establish a compact jet under driving pressures up to 0.8 MPa (in performance tests up to 2.5 MPa) and to study its interaction with different substratum materials. The molten corium was simulated by an alumina-iron thermite melt. Using a revolving mechanism for the substratum samples, the interaction with both melt phases could be studied separately. The gas break-through was avoided by sharply reducing the driving pressure at the end of the melt ejection process.

After a series of performance tests with water and thermite melt on the jet behaviour, seven interaction tests (KJ02 to KJ08) were carried out. The released total amount of melt per test was up to 160 kg. Driving pressures were varied from 0.3 to 0.8 MPa. Two different types of concrete were used as substratum materials, namely construction concrete and borosilicate glass concrete. Among others, the erosion rates in depth and the volume erosion were studied.

In the frame of the KAJET programme, a data base has been generated for model development and testing. Two test series with different concrete types, different driving pressures and different melt phases are now available. In KJ02, KJ03, KJ04 and KJ08, siliceous construction concrete was used at pressures of 0.3 / 0.5 / 0.8 MPa. In KJ05, KJ06, and KJ07, borosilicate glass concrete was eroded at 0.4 / 0.5 / 0.8 MPa. The erosion rates in depth for iron are generally bigger than for oxide, and the rates for construction concrete are bigger than for borosilicate glass concrete. For construction concrete, these rates (in mm/s) are between 8.9 and 11.2 (iron) and between 4.5 and 10 (oxide). For borosilicate glass concrete, the rates are between 5.2 and 8.0 (iron) and 2.8 and 5.1 (oxide), respectively. In all cases the erosion rate increases with increasing driving pressure. However, volume erosion rates are similar for iron and oxide, or may be even larger for oxide.

Theoretical analysis and interpretation has been performed in close cooperation with Ruhr-Universität Bochum and is reported separately. The melting of the structure material by the heat load of the impinging jet has been identified as the decisive mechanism for erosion.

Zusammenfassung

KAJET-Experimente mit druckgetriebenen Schmelzestrahlen und deren Wechselwirkung mit Beton

Im Falle eines punktuellen Versagens des Reaktordruckbehälters kann der Schmelzeausstoß kurzzeitig als kompakter Strahl erfolgen, gefolgt von einer dispergierenden Freisetzung nach dem Gasdurchbruch. Die KAJET-Experimente bezogen sich auf die kurze Anfangsphase als kompakter Strahl. Gegenstand der Experimente war zunächst, einen möglichst kompakten Schmelzestrahl bei treibenden Drücken bis 0,8 MPa zu erzeugen (in Vorversuchen bis 2,5 MPa) und dann die Wechselwirkung des auftreffenden Strahls mit unterschiedlichen Betonsorten zu untersuchen. Die Kernschmelze wurde dabei durch eine Aluminiumoxid-Eisen-Thermitschmelze simuliert.

Mit Hilfe eines Drehmechanismus für die exponierten Betonproben konnten die beiden Schmelzephasen (Metall und Oxid) getrennt behandelt werden. Der Gasdurchbruch wurde durch schnelle Reduktion des Treibdruckes am Ende des Schmelzeausstoßes vermieden.

Nach einer Reihe von Vorversuchen mit Wasser und Thermitschmelze zum Strahlverhalten wurden sieben Experimente zur Wechselwirkung mit Beton durchgeführt (KJ02-KJ08). Dabei wurden bis zu 160 kg Schmelze pro Experiment eingesetzt. Die Treibdrücke wurden variiert von 0,3 bis 0,8 MPa. Als Probenmaterial wurde Konstruktionsbeton und Borosilikatglasbeton verwendet. In erster Linie wurden die Erosionsraten gemessen, bezogen auf die Tiefe und das Volumen.

Im Rahmen des KAJET-Programms wurde eine Datenbasis für die Modellentwicklung erzeugt. Zwei Versuchsreihen mit unterschiedlichen Betonsorten, verschiedenen Treibdrücken und verschiedenen Schmelzephasen stehen nun zur Verfügung. In KJ02, KJ03, KJ04 und KJ08 wurde silikatischer Konstruktionsbeton erodiert bei Treibdrücken von 0,3/0,5/0,8 MPa, In KJ05, KJ06 und KJ07 wurde Borosilikatglasbeton erodiert bei 0,4/0,5/0,8 MPa. Die Tiefenerosionsraten für Eisenstrahlen sind generell höher als für Oxidstrahlen, und die Raten für Konstruktionsbeton sind generell höher als für Borosilikatglasbeton. Für Konstruktionsbeton liegen die Erosionsraten (in mm/s) zwischen 8,9 und 11,2 (Eisen) sowie zwischen 4,5 und 10 (Oxid). Für Borosilikatglasbeton liegen die Raten zwischen 5,2 und 8,0 (Eisen) sowie 2,8 und 5,1 (Oxid). In allen Fällen steigen die Raten mit dem Treibdruck an. Die Raten der Volumenerosion sind allerdings bei beiden Schmelzephasen ähnlich oder für Oxidstrahlen sogar höher.

Modelltheoretische Untersuchungen und Interpretation der Ergebnisse erfolgten in enger Zusammenarbeit mit der Ruhr-Universität Bochum. Über diese Arbeiten wird an anderer Stelle berichtet. Das Aufschmelzen des Strukturmaterials infolge Wärmeeintrags durch den auftreffenden Schmelzestrahl wurde als der entscheidende Mechanismus identifiziert, der zur Erosion führt.

Contents:

List of Tables

List of Figures

1 Introduction

In the event of a postulated core melt-down accident, hypothetical scenarios are considered in which the reactor pressure vessel (RPV) fails and the core melt is discharged into the reactor cavity /1/. In this context, efforts are currently directed towards long-term retention and cooling of ex-vessel corium in the containment /2/. Core catcher concepts are under investigation that should prevent basemat erosion and stabilize and control the corium within the containment /3/. Various modes of corium release out of the RPV may be envisaged: e.g., release by gravity or under overpressure resulting in low or high flow rates, respectively, liquid melts carrying solid debris, and intermittent melt discharge. Analyses within the French GAREC group /4/ predict pressure increases of up to 2 MPa inside the RPV. In case of wall failure, melt may be released as a compact jet causing erosion in the substratum material. However, the time of release as a compact jet is expected to be rather short (a few seconds) and will be terminated by gas break-through and dispersion of the melt. The melt will consist of an oxidic phase and of a metallic phase. Both phases are expected to separate in-vessel due to their differences in density. After wall failure, it is likely that both phases are discharged separately in a sequence. A sketch of the scenario is shown in Fig. 1.1.

Generally, the degree of erosion is determined by physical phenomena such as mechanical and thermal stresses caused by the impact of the jet and heating of the substratum, and physico-chemical interaction including melting of the substratum. Parameters that influence erosion are the driving pressure, speed and temperature of the jet, the duration of interaction, the compositions (physical properties) of the jet as well as of the substratum material, and the angle of inclination of the jet.

Following the GAREC needs, the ex-vessel situation should be addressed by experiments with oxidic and metallic jets on ceramics (zirconia and others) and on different concrete types. It is emphasized that the situation with oxide on ceramics can be represented by a molten alumina jet, provided that the temperature is high enough so that alumina is able to dissolve the ceramics and the duration is long enough to ensure a remelt of a solid alumina crust and a sufficient time for interaction. The jet velocity should be around 10 m/s for about 1 MPa driving pressure, the temperature should be around 2200 °C, and the duration should be at least 10 s. Concrete is expected to ablate faster than ceramics, so the duration may be somewhat shorter. Concerning metallic jets, the conclusion from new studies is that the temperature of the metal melt pool layer in contact with the RPV is less than the oxidic pool. So, the main interest is oriented to metal jet-concrete interactions at temperatures somewhat below 2000 °C. Again, the jet duration should be long enough to observe a significant erosion for model validation.

At Forschungszentrum Karlsruhe, an experimental programme named KAJET has been performed to investigate features of a pressurized melt jet and mode of interaction with substratum materials. As for erosion, compact melt jets, rather than a spray-type melt release, are regarded to be most effective. In the KAJET experiments, simulant melt materials (iron and alumina) were applied instead of corium. The melt was generated by a thermite reaction. Emphasis was placed on the needs listed above, i.e. separate investigation of metallic and oxidic jets, variation of the substratum materials, driving pressures of the order of 1 MPa,

melt temperatures in the range of 2200 °C, and durations of several (up to 10) seconds. The experiments provided, besides general information about erosion processes, a data base for the validation of computer codes (or, if possible, simplified correlations) which then are able to recalculate the experiments and transfer the results to reactor conditions.

The KAJET programme has been divided into three steps, namely performance tests with water, performance tests with thermite melt, and erosion tests with thermite melt. Due to severe financial and personnel shortages, the programme has been restricted to the investigation of two types of concrete, namely construction concrete and borosilicate glass concrete, and to driving pressures (for the erosion tests) from 0.3 to 0.8 MPa. The maximum amount of melt was 160 kg. The programme was terminated by the end of 2002. Unfortunately, it was not possible to investigate the interaction with ceramics as substratum material. Preliminary results have already been presented in refs. /5/ and /6/.

The erosion tests are included as a work package within the ECOSTAR project of the Fifth EU Framework Programme. To gain valuable and detailed information on the whole field of ex-vessel core melt stabilization research (from melt release to melt retention), the reader is referred to references on this project, such as /7, 8/.

The present report will focus on the experimental part of the programme. Theoretical analysis and interpretation has been performed in close cooperation with Ruhr-University Bochum (RUB) and is reported separately /9, 10/. It is also reported in literature on the ECOSTAR project.

2 Performance tests with water

To perform the tests, it is necessary to generate a pressure-driven well-defined liquid jet. Therefore, an ejection nozzle is needed which produces a jet which remains rather compact between nozzle exit and surface of impact sample (of the order of 200 mm).

Important quantities of nozzle design, as shown in Fig. 2.1, are the inlet diameter d_i, the outlet diameter d, the angle of contraction α, and the length of the exit pipe L. An outlet diameter d=12 mm has been chosen in all the test. This is small enough to guarantee a sufficiently long ejection time and wide enough to prevent plugging in case of thermite discharge. Important quantities to characterize the jet are, besides d, the jet velocity u and the kinematic viscosity ν as a material property. A combination of these quantities is the Reynolds number

$$Re = ud/\nu$$

Correlations between L, d, and Re for turbulent conditions are reported in the literature /11, 12/:

- $L/d=0.693 \cdot (Re)^{0.25}$ (Latzko)
- $L/d=14.25 \cdot \log_{10}Re - 46$ (Bowlas and Brighton)

In our water tests, two different exit pipe lengths L were installed, namely 0.184 m (Latzko) and 0.370 m (Bowlas and Brighton). They were calculated for u=20 m/s, as recommended by GAREC, which corresponds to $Re = 2.4 \cdot 10^5$. (But note: The length in the erosion tests was much smaller for a better representation of the actual leak!).

An inlet diameter d_i=25 mm has been used in all our water tests. Nozzles with three different angles, α=30°/45°/60°, were selected for the tests and combined with the two different exit pipe lengths. Flow resistance coefficients for such nozzles are reported in the literature /11, 12/.

Finally, it is necessary to have a correlation between the driving pressure in the upper reservoir p and the jet velocity u. This correlation includes the pressure loss in the nozzle and in the exit pipe:

$$p=u^2 \cdot \rho /2 + p_o + \Delta p_p + \Delta p_n$$

with ρ=liquid density, p_o= ambient pressure, Δp_p= pressure loss in the pipe and Δp_n= pressure loss in the nozzle. Correlations to calculate the pressure losses are

$$\Delta p_p=\lambda \cdot (L/d) \cdot (\rho/2) \cdot u^2$$

$$\Delta p_n=\zeta \cdot (\lambda/2) \cdot u^2$$

with $\lambda=1/[1.72 - 2 \cdot \log (2k_s/d)]^2$, where k_s is the average pipe roughness and ζ is the nozzle resistance coefficient. These numbers have to be taken from literature.

As an example for our case, using $k_s/d=0.02$ and $\zeta=0.08$, a driving pressure of 0.5 MPa is necessary to achieve a jet velocity of u=20 m/s. In that case, the pressure loss in the pipe is 0.151 MPa, and 0.016 MPa in the nozzle.

A sketch of the experimental setup is shown in Fig. 2.2. To gain comparable results, the water reservoir was always filled with the same amount of water (14 liters). The water was ejected by a well-defined driving pressure. The water jet was observed by a video camera. Pressures and other quantities were recorded using a data logger. The distance between nozzle exit and target was 750 mm. However, as mentioned above, the focus of the tests was to determine the jet enlargement, diameter D, at a distance of 200 mm. A photo of a typical water jet is shown in Fig. 2.3.

Eighteen tests were performed, as listed in Tab. I. Parameters, as described above, were the length of the exit pipe and the angle of contraction. The driving pressure was 0.5, 1.5 and 2.5 MPa, respectively. The corresponding jet velocity was calculated. The jet enlargement D/d was determined from video films. A continuous increase of the jet diameter from exit to target is observed. Of course, this increase rises with driving pressure. Very ‘clean’ jets were produced at low pressure, whereas mist generation was observed at higher pressures. The angle of contraction and the pipe length turned out to be of minor influence. Some preference exists for a 30° contraction angle. (But note: to represent a realistic leak in the RPV, a larger angle should be used). Concerning the pipe length, even shorter pipes may be used in the follow-on thermite melt tests to prevent freezing and plugging. (But note: nozzle erosion, not plugging, turned out to be a problem in the thermite tests).

3 Performance tests with thermite melt

3.1 Overview

The generation of an iron-alumina thermite melt is a well-established technique. According to the general equations

$$8Al + 3Fe_3O_4 \rightarrow 4Al_2O_3 + 9Fe + 3730\ J/g$$

$$216\ g + 696\ g \rightarrow 408\ g + 504\ g + 3.40\ MJ$$

a hot melt of iron and alumina is generated at a temperature of typically 2300 °C. Lower temperatures are achieved by using non-stoichiometric mixtures. Both components (metallic and oxidic) separate by gravity. The density of iron is near 6400 kg/m^3, of alumina near 2900 kg/m^3 at that temperature. They may be released from the source in a sequence (first metal, then oxide) or partly retained in the source, if the experiment is restricted to one component only (typically oxide as a simulant of corium). An important issue of the tests was to generate rather compact melt jets for both components with impact velocities up to 25 m/s, using the knowledge from the preceding water tests. Results from calculations for water, alumina, and iron are listed in Tab. II. The generated volume of the alumina melt is about twice the volume of iron, and the difference in jet velocity is about a factor of 1.6. So, the alumina jet should have a longer time duration than the iron jet. In reality, this is not the case due to nozzle erosion.

Seven performance tests, named VJ01 to VJ07, were carried out in a facility which is shown in Fig. 3.1. It consisted mainly of a thermite melt generator with ejection nozzle and a sand bed 1.7 m below to catch the released melt. Protective concrete rings were installed between generator and sand bed, with small openings for video observation. A 10 kg source was used in VJ01 to VJ04, a 20 kg source later on. The melt was ejected under argon pressure. A ventilated off-gas system was installed to remove the smoke and to improve the visibility. Another performance test, named KJ01, was finally performed in the ‘large’ KAJET erosion test facility.

3.2 Performance tests VJ01 to VJ04

The boundary conditions were similar in all these tests. The parameters were mainly adjusted to the physical properties of the oxide melt. In most cases, nozzles fabricated from zirconia were used. Dimensions of the nozzle system were: α=30°, L=110 mm, d=12 mm. The driving pressure was 1.6 MPa to achieve an impact velocity of 25 m/s. Calculated release times are 0.4 s for iron and 0.6 s for oxide. The melt temperature was near 2300 °C. From VJ02 on, horizontal wire grids were mounted 300 mm and 600 mm below the nozzle exit to gain information on the maximum jet enlargement under bad visibility conditions. From VJ03 on, these grids were additionally equipped with melt detectors to get a time resolution.

An evaluation of VJ01 was not possible due to bad visibility by smoke generation. In addition, post-test investigations showed a rupture of the nozzle exit pipe.

In VJ02, the ventilation system was improved and the melt temperature slightly reduced (2260 °C). A strongly expanding jet was observed. According to the molten part of the wire grid, the expansion was from 12 mm to 360 mm at a distance of 600 mm. Again, problems with the stability of the exit pipe occurred.

In VJ03, the nozzle was fabricated from stainless steel instead of zirconia due to delay in delivery. The driving pressure was retarded in such a way that the iron was released mainly under gravity. Under that condition, a compact jet was observed. However, the jet expanded immediately under the influence of driving pressure. Post-test investigation showed an erosion of the nozzle diameter from 12 to 25 mm. Due to this, the iron was released faster than expected, the application of driving pressure was too late, and only 1.1 MPa pressure were reached for the oxide. The maximum enlargement at 600 mm was 190 mm.

In VJ04, the application of the driving pressure started at the instant of iron release, but with a linear increase from ambient pressure to 1.6 MPa within 1 s. Thus, the melt was ejected under a continuously increasing pressure. An enlargement of the jet, super-proportional to the pressure, was observed. Gas break-through near the end of ejection had an important influence.

3.3 Performance tests VJ05 and VJ06

A 20 kg melt generator was used in these tests. In addition, the iron was retained in the generator by a technique which was successfully established in the PREMIX experiments on melt-water interaction /13/. So, the tests were performed with oxide melt only, and almost twice the release time. The increase of driving pressure from gravity conditions to 1.5 MPa could be extended to 1 s. After a short hold (0.1 s), the pressure was reduced to gravity again within 0.5 s in order to avoid the disturbing gas break-through at the end of release. To gain information on the jet enlargement with time resolution, a horizontally moveable wire grid was installed 300 mm below the nozzle exit instead of a fixed grid. It was mounted on a sledge and moved in horizontal direction, perpendicular to the jet, during melt release. By this, the jet produced a ‘footprint’ as a longish hole in the grid which could be correlated to the pressure-time history (see Figs. 3.2 and 3.3).

Both tests delivered valuable results on the jet behaviour during the phase of pressure increase. The molten area of the grid had a width of about 40 mm from 0.2 to 0.4 MPa and almost constantly 70 mm from 0.4 to 1.5 MPa. So, the jet may be considered as relatively compact (see also Fig. 3.4). A gas break-through with disturbing effects was avoided. The much better visibility may be related to the fact that most of the smoke in the previous tests was caused by condensation aerosol of evaporated iron.

3.4 Performance test VJ07

The aim of VJ07 was to investigate the behaviour of both melt components, iron and oxide, under similar conditions as in the two tests before. The melt generator was modified to a capacity of 40 kg. The argon pressurizing system had to be modified according to the new conditions. The moveable grid was installed and operated in a similar way as before.

The test delivered valuable results on the behaviour of both melt jets in relation to the driving pressure. Unlike VJ01 to VJ03 with early nozzle failure, the ejection of the iron jet could be observed and recorded for the first time in our tests. The jet was very compact, practically independent of the driving pressure. The oxide was less compact, and small splashes were observed, probably due to expanding gas bubbles which were included in the melt.

3.5 Performance test KJ01

The new KAJET facility designed for the erosion tests was built in 1998. Various types of melt generators may provide total melt masses of up to 300 kg and driving pressures of up to 2.5 MPa. The melt jet is released downward into a vessel that is 1.1 m in diameter and 1.9 m in height. The bottom of the vessel is covered by a layer of gravel and sand. The pressure inside the vessel can be raised up to 0.3 MPa (see chapter 4.1 for a sketch and more details). In searching designs of appropriate nozzles, advantage was taken of previous work done at other laboratories on wall ablation and hole enlargement. For example, experiments with iron-alumina melt jets were performed at Sandia National Laboratories /1/, experiments with salt melts and PbO-B_2O_3 oxidic melt mixtures at PNC, Japan /14/, and at the Stockholm KTH Institute of Technology /15/, respectively. In some cases, test plates were used whose materials had much lower melting points compared with the RPV wall material. Fig. 3.5 shows two typical results of these tests.

The performance tests were begun with water and continued with thermite melt. The latter were performed in a preliminary test facility (VJ01 –VJ07) as well as in the new KAJET facility (KJ01). Beginning with rather long nozzles made from varying materials, we finally installed and tested short nozzles which were able to generate compact jets and which reflect the above geometry (Fig. 3.5). The last performance test, KJ01, aimed at checking jet formation in the new facility. In doing so, a nozzle was used whose geometry resembles to that of a hole in an RPV wall expected to be generated by melt through. Otherwise, the KJ01 test conditions agree with those of the preceding VJ07 test. To determine the jet diversion, the moveable wire grid was installed as before in VJ05 to VJ07. The jet produced a “footprint” as a longish hole in the grid which could be correlated to the pressure-time history. Roughly, the width of the iron jet was about one half of the width of the oxide jet (see Fig. 3.6 and 3.7).

Conditions and results of VJ05, VJ06, VJ07 and KJ01 are listed in Tab. III. A summary of the water tests is listed as well. The jet diversion for water is extrapolated from 200 mm to 300 mm.

4 Erosion tests

4.1 Facility

As already mentioned in chapter 3.5, a new and larger facility was built to perform the erosion tests. The design of this facility was such that various types of melt generators could provide total melt masses of up to 300 kg under driving pressures up to 2.5 MPa. The test vessel had a diameter of 1.1 m and a depth of 1.9 m. It was designed for system pressures up to 0.3 MPa.

The melt generators were equipped with ‘short’ nozzles as described in chapter 3.5. In most experiments, iron melt and oxide melt were released in a sequence for impact on substratum samples. Typically, these samples had a surface area of 320 x 200 mm and a height of 100 mm. Each plate was instrumented with thermocouples in horizontal levels to measure the progression of erosion.

A revolving mechanism was installed to allow separate studies of both melt phases. For that purpose, two sample plates with identical dimensions and instrumentation were installed under a 90° angle on a carrier device.

Usually, the first melt component (iron) was ejected on sample 1. Shortly before the end of iron release, the plate carrier was turned by 90° within about one second. During that time, the melt changed to oxide, and the oxidic jet was ejected on sample 2. In a later stage of the programme, another 90° turn followed at the end of oxide release to avoid long-term melt-concrete reactions with oxidic melt remaining in the cavity of the sample.

A sketch of the facility is shown in Fig. 4.1. The arrangement with melt source, melt jet and revolving plate carrier is schematically shown in Fig. 4.2. A photograph of the facility is shown in Fig. 4.3, and a photograph of the revolving carrier in Fig. 4.4. In Tab. IV, information on both concrete types is presented. Fig. 4.5 shows the nozzle made from zirconia and instrumented with NiCr-Ni thermocouples. As mentioned in chapter 3, the diameter of the nozzle increased by erosion from 12 mm to about 25 mm. For the evaluation of the experimental results it is important to know the time dependency of the erosion. Therefore, thermocouples are used as detectors in different distances from the center line.

As already mentioned in chapter 1, severe shortages in funding occurred during the course of the programme, mainly caused by political directions and nuclear phase-out plans in Germany. So, the programme was restricted to two types of concrete samples (construction concrete and borosilicate glass concrete), to maximum melt masses of 80 kg per component, and to maximum driving pressures of 0.8 MPa. The programme was also restricted to seven erosion tests only.

4.2 Erosion test KJ02

The first erosion test, KJ02, was performed in March 1999. Test conditions are listed in Table V. Still, a rather small melt source was used, delivering about 20 kg of melt for each

component. The schematic (Fig. 4.2) helps to explain how the test was conducted. The time scale begins with the start of ejection. The first melt component to be ejected on sample 1 was iron. Shortly before the end of iron release, the plate carrier was turned by 90° within one second. During that time, the melt changed to oxide as the component to be ejected on sample 2. The test plates, 100 mm thick, consisted of ordinary concrete made from cement, sand and pebbles (0 – 32 mm), and water at a mass ratio of 1:5.5:0.4, respectively. Each plate was instrumented with 25 thermocouples. These were arranged in five horizontal levels at distances of 5 to 25 mm, from the upper surface. In each level, the thermocouples were crosswise arranged with respect to the intended centre of impact of the jet. The melt temperature was measured by a pyrometer. A CCD film camera was installed to observe the melt jet, but did not deliver pictures of satisfying quality. The camera was destroyed after one to two seconds by heat and/or by melt impact.

Figure 4.6 (a, b) shows the size of erosion in both plates. The cuts were made along the centre line across the narrow sides laying bare three of the thermocouple channels embedded in the concrete. Obviously, impact of the jet and erosion in the iron case did not occur in the centre but some 25 mm apart. The hole was rather cylindrical, the depth (25 mm) being about half the width. The cut in the “oxide” plate does not show the maximum depth of erosion which was 15 mm, see Table V. Nonetheless, it shows that the width to depth ratio was much larger than in the iron case. The eroded volume was 45 ml for iron and 40 ml for oxide. Crusts, up to one millimeter thick, were found at all surfaces contacted by melt.

Progression of erosion is visible in the temperature traces, where signals of thermocouples have been chosen that were located near by the centre of erosion found after the test. Increase in temperature indicates the approach, a very steep rise ending in a value of 1600 °C the arrival of the melt (see Fig. 4.6 c, d). The instants of the latter events have been used to draw the actual depth of erosion as a function of time, where the location in the horizontal plane is taken as a parameter. One can state, as a first result, that the maximum initial rates of erosion are larger with iron (around 11 mm/s) than with oxide (7.5 mm/s). The average rates are 8.9 and 4.5 mm/s, respectively.

Inspection of the nozzles after the test showed that the internal surfaces had been eroded so that the internal diameters were enlarged from 12 to 22 mm.

4.3 Erosion test KJ03

The second erosion test, KJ03, was performed in September 1999. Compared to KJ02, a larger melt source was installed, to deliver about 60 kg of melt per component, and the driving pressure was enlarged to 0.5 MPa. The test plates were instrumented with thermocouples in five horizontal levels at distances of 5 to 60 mm from the upper surface. Otherwise, conditions were similar to KJ02 (see Tab. V).

Unfortunately, the plate carrier failed, and both melt components were released onto sample 1. The cut of the eroded plate shows a rather cylindrical hole (see Fig. 4.7). Crusts, one to two millimetres thick, were found at the eroded surfaces. Considering the total volumes of erosion, one can state that the erosion was significantly larger compared to KJ02. This result is primarily due to the larger melt mass, but also to the larger driving pressure.

Inspection of the nozzle after the test showed an enlargement of the internal diameter from 12 to 24 mm due to erosion.

4.4 Erosion test KJ04

KJ04, performed in March 2000, was a continuation of the previous tests KJ02/03. Siliceous concrete was used as before. However, to study the nozzle erosion, the test was limited to the oxidic phase of the melt only. To achieve this, the melt source had to be modified in order to retain the iron melt in a separate annular chamber. This technique has been successfully developed for application in the former PREMIX fuel-coolant interaction tests /13/. The released amount of oxidic melt in KJ04 was 83 kg, compared to 21 and 60 kg in KJ02/03. Thus, with driving pressure 0.5 MPa, the duration of ejection was 10 s, compared to 6.3 and 7 s in the previous tests.

In Table V, the test conditions and the obtained erosions are summarized. The progression of erosion was measured by the destruction of thermocouples. The average erosion rate in depth was about 4.8 mm/s and was proportional to the time. The eroded volume was about 360 ml (see Fig. 4.8). The nozzle erosion was from 12 mm diameter initially to 24 mm at the end of melt release. This indicates that an extension of melt ejection beyond 10 s may lead to nozzle destruction and severe problems in data interpretation. Test results may be compared to KJ02, especially the oxidic part. Obviously, the erosion rates are very similar, although the eroded volume in KJ04 is much bigger.

4.5 Erosion test KJ05

In KJ05, performed in August 2000, the concrete type has been changed. Borosilicate glass concrete (see Tab. III) was studied for the first time in our tests. Both melt phases, iron and oxide, were released, using a total mass of 104 kg, divided into 49 kg of iron and 55 kg of oxide. The driving pressure was 0.5 MPa. Both melt phases were released on separate concrete samples, using the revolving mechanism. This time, the mechanism worked properly after improving the coupling to the motor which caused malfunction in KJ03. In addition, the nozzle exit was equipped with a separate zirconia plate carrying thermocouples to measure the nozzle erosion at various radial distances. In Table VI, the test conditions and the obtained erosions are summarized. The average erosion rate in depth was about 6.5 mm/s for iron and 3.8 mm/s for oxide. The erosion was proportional to the time. Fig. 4.9 shows a vertical cut of the samples along the short side. The iron melt jet eroded the sample more deeply (33 mm) than the oxide melt jet (23 mm), but the oxide eroded a larger amount of the concrete (iron 39 ml, alumina 120 ml). There are indications that the erosion rates for borosilicate glass concrete are smaller than for construction concrete (compare to KJ02).

The nozzle diameter increases during the melt release by thermal, chemical and mechanical influences. For the operation sequence of the experiment it is important to know the duration of the individual melt phases. Therefore, the erosion of the nozzle was detected by thermocouples. During the iron release, the nozzle diameter grew from 12 to 14.6 mm. The following oxidic melt extended the diameter to the final size of 25.4 mm. It is evident that a further increase of the melt mass or an extension of the release duration in our tests is limited, because the erosion rises super proportionally.

4.6 Erosion test KJ06

KJ06 was performed in February 2001. Borosilicate glass concrete was used as before in test KJ05. The released amount of melt was 115 kg. Both melt phases (iron: 54 kg, oxide: 61 kg) were released on separate concrete samples, using the revolving mechanism. Thus, with driving pressure 0.4 MPa, the duration of impact was 7.3 s (iron) and 4.6 s (oxide). In Table VI, the test conditions and the obtained erosions are summarized. Fig. 4.10 shows the cavities in the concrete formed by jet erosion. The cut was made along the long side. The progression of erosion was measured by the destruction of thermocouples in all experiments. A strong gas flame occurred during the oxide interaction (reason still unknown). The average erosion rate in depth was about 5.2 mm/s (iron) and 2.8 mm/s (oxide) and was nearly proportional to the time. The eroded volume was about 12.6 ml (iron) and 12.8 ml (oxide).

The nozzle outlet was instrumented by thermocouples to measure the erosion over time. Unfortunately, the thermocouples were destroyed by the melt during the start of the release (the reason is unclear). The nozzle erosion was from 12 mm diameter initially to 28 mm at the end of melt release.

Test results may be compared to KJ05 with similar test conditions. The driving pressure of KJ06 (0.4 MPa) was smaller than in KJ05 (0.5 MPa). Therefore, the duration of the iron melt jet was longer and eroded a deeper cavity. Due to the longer duration of the melt, the nozzle diameter grew up to a bigger diameter than in KJ05 and the oxide melt was released faster. Therefore, the duration and the erosion depth is smaller than in KJ05.

4.7 Erosion test KJ07

KJ07 was a continuation of the previous tests KJ05 and KJ06. It was performed in August 2001. Both melt phases, iron and oxide, were released, using a total mass of 152 kg, divided into 71.5 kg of iron and 80.5 kg of oxide. The driving pressure, 0.8 MPa, was twice as high as in KJ06. In Table VI, the test conditions and the obtained erosions are summarized. The average erosion rate in depth was about 8 mm/s for iron and 5.1 mm/s for oxide. The erosion was nearly proportional to the time. Fig. 4.11 shows a vertical cut of the samples along the long side. The iron melt jet eroded the sample more deeply (45 mm) than the oxide melt jet (20 mm). But the eroded volume is similar, Fe: 95 ml, oxide: 110 ml. The signals of the thermocouples of both samples the erosion depths in both samples and the pressure vs. time are also shown in Fig. 4.11.

For the operation sequence of the experiment it is important to know the duration of the individual melt phases. Therefore, the erosion of the nozzle was detected by thermocouples. Fig. 4.12 shows the experimental data and the post calculation of the erosion over time. During the iron release, the nozzle diameter grew from 12 to 15.5 mm. The following oxidic melt extended the diameter to the final size of 29 mm. Again, a gas flame occurred during the oxide interaction. It was even stronger than in KJ06.

4.8 Erosion test KJ08

KJ08 was performed in March 2002. Silicous concrete was used as before in the tests KJ02-KJ04. The released amount of melt was 159.5 kg. Both melt phases (iron: 75 kg, oxide: 84.5 kg) were released on separate concrete samples, using the revolving mechanism. Thus, with driving pressure 0.8 MPa, the duration of impact was 5.8 s (iron) and 2.9 s (oxide).

In Table V, the test conditions and the obtained erosions are summarized. Fig. 4.12 shows the cavities in the concrete formed by jet erosion. The cut was made along the short side of the sample. The progression of erosion was measured by the destruction of thermocouples. The erosion depth and the pressure vs. time are shown in Fig. 4.17. The average erosion rate in depth was about 11.2 mm/s (iron) and 10 mm/s (oxide), and the erosion was proportional to the time. The eroded volume was about 180 ml (iron) and 95 ml (oxide).

The nozzle outlet was instrumented by thermocouples to measure the nozzle erosion over time. After the re-examination it was noticed that the nozzle was strongly washed out locally in the region of the thermocouples. Therefore the measured erosion rate is too large and does not agree with the actually erosion of the nozzle. To be able to characterize the melt discharge, an erosion rate similar to earlier experiments is assumed which was measured correctly.

5 Remarks on theoretical work

The erosion of structures in the reactor pit occurs in a complex manner by thermal, chemical and mechnical effects: Melting of concrete/substratum, chemical decomposition of the structure material and forces from the jet to the structure.

The erosion of the concrete structures by impinging metallic and oxidic melt jets is also controlled by the heat transfer. The thermal interaction between jet and structure can be classified into five idealized reference cases:

In the 1st case, it is assumed that no phase change of the jet fluid or the structure material occurs. In the 2nd, the jet fluid is assumed to freeze and to form a crust on top of the structrure. It is equally possible that, as depicted in the 3rd case, the structure material melts and forms a layer between the solid structure and the jet fluid. A special case of this situation is the fast removal of molten structure material with the jet flow so that no well defined melt layer is formed (4th case). As a 5th case, depending on the temperature at the jet-structure interface, it can also be thought of a simultaneous freezing of the corium and melting of the stucture.

The investigations at RUB showed that the erosion of concrete structures is mainly governed by the thermal erosion process due to the heat transfer from the jet. Mechanical and chemical processes have a minor influence.

Idealised reference cases for the heat transfer have been analysed and necessary Nusselt number correlations – based on the erosion for metal structures – have been discussed. Criteria for a Nusselt number correlation optimised for concrete structures regarding the influence of geometry and material properties could be formulated. Related to the KAJET experiments, a correlation for metallic and oxidic melt jets has been set up.

In relation to future large pressurized water reactors, four scenarios for a jet-like melt ejection from a breach in the RPV-bottom onto structures of silicious concrete have been investigated, where, based on a density-influenced layering of metallic melts over oxidic phases inside a melt pool, the focus was on the ejection of the oxidic melt. The obtained data could be compared to pool configurations due to results of erosion codes performed with similar boundary conditions. Regarding silicious concrete instead of sacrificial as a first approximation, it is shown that the melt jet can deliver significant erosion depths.

For an investigation of the influence of mechanical and chemical erosion mechanisms on the structure erosion by melt jets it is suggested to further perform single effects experiments and to investigate the properties of concrete under melting conditions more detailed.

A more extensive description of the RUB-LEE analysis of the structure ablation by impinging melt jets supplemented by an extensive literature list is given in Refs. /9, 10/.

6 Summary

In the event of a postulated core melt-down accident, hypothetical scenarios are considered in which the reactor pressure vessel (RPV) fails and the core melt is discharged into the reactor cavity.

In case of a localized RPV failure, the melt expulsion into the cavity may be as a compact jet for a short period, followed by a dispersed release after gas break-through. The KAJET experiments were related to the short initial phase of a compact jet. The main objective of the experiments was, according to conditions formulated by the French GAREC group, to establish a compact jet under elevated driving pressures and to study its interaction with different substratum materials. The molten corium was simulated by an alumina-iron thermite melt. Using a revolving mechanism for the substratum samples, the interaction with both melt phases (metallic and oxidic) could be studied separately. The gas break-through was avoided by sharply reducing the driving pressure at the end of the melt ejection process.

After a series of performance tests on the jet behaviour with water and thermite melt under driving pressures up to 2.5 MPa, seven interaction tests (KJ02 to KJ08) were carried out. The released total amount of melt per test was up to 160 kg. Driving pressures were varied from 0.3 to 0.8 MPa. Two different types of concrete were used as substratum materials, namely construction concrete and borosilicate glass concrete. Among others, the erosion rates in depth and the volume erosion were studied. Experiments with other types of substratum materials (especially ceramics such as zirconia) were foreseen but not carried out due to severe shortages in the programme caused by external reasons.

Following correlations from literature, the performance tests were carried out with rather long nozzle exit pipes to generate a compact jet. But finally it turned out that much shorter pipes, corresponding to the shape of an actual RPV leak, could be used as well. Nozzles fabricated from zirconia were used in most cases. A plugging of the nozzle did never occur. However, a significant erosion of the nozzle during melt release was observed, typically from 12 to 25 mm in diameter. The main part of the erosion occurred during release of the oxidic phase.

The GAREC needs were used as a guideline for the selection of the experimental parameters. The metallic phase and the oxidic phase of the melt were treated separately in most cases. Driving pressures approaching 1 MPa were established as well as impact velocities in the range of 10 m/s. The duration of the impact was limited by the erosion of the nozzle. Values between 3 and 10 s were achieved, long enough to study the progression of the erosion and to determine erosion rates. Melt temperatures were up to 2150 °C. Of course, it was not possible to treat the two melt phases under different temperatures.

In the frame of the KAJET programme, a data base has been generated for model development and testing. Two test series with different concrete types, different driving pressures and different melt phases are now available. In KJ02, KJ03, KJ04 and KJ08, siliceous construction concrete was used at pressures of 0.3 / 0.5 / 0.8 MPa. In KJ05, KJ06, and KJ07, borosilicate glass concrete was eroded at 0.4 / 0.5 / 0.8 MPa. The erosion rates in depth for iron are generally bigger than for oxide, and the rates for construction concrete are bigger

than for borosilicate glass concrete. For construction concrete, these rates (in mm/s) are between 8.9 and 11.2 (iron) and between 4.5 and 10 (oxide). For borosilicate glass concrete, the rates are between 5.2 and 8.0 (iron) and 2.8 and 5.1 (oxide), respectively. In all cases the erosion rate increases with increasing driving pressure. However, volume erosion rates are similar for iron and oxide, or even larger for oxide. A summary is presented in Tab. VII. The increase of the melt jet diameter due to nozzle erosion has to be considered in the analysis of the tests.

The theoretical investigations were aimed to describe the KAJET results and to allow the application to reactor conditions. They were performed by RUB and are reported separately. The melting of the structure material by the heat load of the impinging jet has been identified as a decisive mechanism.

7 Acknowledgement

We thank our colleagues from the former section IRS-4 of FZK for their contributions to the experiments.

The very fruitful cooperation with our colleagues from Ruhr-Universität Bochum on evaluation and theory is highly acknowledged. Especially, we thank Dr. M.K. Koch and Dr. T. Büscher from RUB/LEE.

Part of the work (experiments KJ04 to KJ08) was performed and supported within the ECOSTAR project of the 5. EU Framework Programme. In this context, we thank Dr. H. Alsmeyer for his management and for valuable discussions.

8 References

/1/ Pilch, M. M., Yan, H., Theofanous, T.G.,
The probability of containment failure by direct containment heating in Zion, NUREG/CR-6075 (1994).

/2/ Azarian, G., Bittermann, D., Eyink, J.,
The overall approach to severe accident mitigation,
in: Kerntechnische Gesellschaft (ed.), The European Pressurized Reactor EPR, Proc., Inforum, Bonn, pp.194-197 (1997).

/3/ Cognet, G., et al.,
Corium Spreading and Coolability (CSC Project),
FISA 1997, EU Research on Severe Accidents, Luxembourg, Nov. 1997, EUR 18258,
pp. 141-151.

/4/ Micaelli, J.C., et al.,
R&D needs related to the core-catcher concept based on corium spreading.
Int. Sem. on Heat and Mass Transfer in Severe Reactor Accidents, Cesme, Turkey (1995).

/5/ Albrecht, G., Jenes, E., Kaiser, A., Schütz, W.,
KAJET Experiments on Pressurized Melt Jets with View to their Interaction with Substratum Materials,
Proc. of the NURETH-9 Conference, Oct. 3-8, 1999, San Francisco, California, USA

/6/ Albrecht, G., Jenes, E., Kaiser, A., Schütz, W.,
KAJET Experiments on Pressurized Melt Jets and their Interaction with Substratum Materials,
Proc. of the Annual Meeting on Nuclear Technology 2000 (Jahrestagung Kerntechnik),
Bonn/Germany, May 2000 pp. 125-130, Inforum GmbH (ISSN 0720-9207).

/7/ Steinwarz, W., et al.,
Ex-Vessel Core Melt Stabilization Research (ECOSTAR),
FISA 2001, EU research in reactor safety, Luxembourg, Nov. 2001, EUR 20281, p. 274-285

/8/ Alsmeyer, H., et al.,
Ex-Vessel Core Melt Stabilization Research (ECOSTAR),
FISA 2003, EU research in reactor safety, Luxembourg, Nov. 2003, Pre-proceedings, 401-406 and Nucl. Eng. Des., Vol. 235 (2005) 271-284

/9/ Büscher, T., Koch, M.K., Unger, H.,
Analysis of the structure ablation by impinging melt jets,
Ruhr-Universität Bochum,
Department of Energy Systems and Energy Economics
Report LEE-18, June 2003; Report ECOSTAR-D13.

/10/ Büscher, T.,
Analyse des Radionunklidquellterms und der Strukturerosion beim Kernschmelzeaustrag aus dem Druckbehälter eines Leichtwasserreaktors,
Dissertation (Thesis), Fakultät für Maschinenbau, Ruhr-Universität Bochum, 2002.

/11/ McCarthy, M.J., Molloy, N.A.,
Review of Stability of Liquid Jets and the Influence of Nozzle Design,
The Chemical Engineering Journal 7, 1974.

/12/ Katayama, S.,
Discharge Coefficients of Fire Nozzles,
J. Basic Eng., Trans ASME 88SD (1966) 706.

/13/ Kaiser, A., Schütz, W., Will, H.,
PREMIX Experiments PM12-PM18 to Investigate the Mixing of a Hot Melt with Water,
Forschungszentrum Karlsruhe, Germany, Scientific Report FZKA 6380, July 2001.

/14/ Saito, M., Sato, K.,Furutani, A., Isozaki, M., Imahori, S., Hattori, Y.,
Melting attack of solid plates by a high temperature liquid jet - effect of crust formation, Nuclear Engineering and Design **121**, pp. 11-23 (1990).

/15/ Dinh, T.N., Bui, V.A., Nourgaliev, R.R.,
Modelling of heat and mass transfer processes during core melt discharge from a reactor pressure vessel,
Nuclear Engineering and Design **163,** pp. 191-206 (1996).

9 Tables

Tab. I: Performance tests with water

Test No.	Length of exit pipe [m]	Nozzle angle [°]	Driving pressure [MPa]	Jet velocity (calc.) [m/s]	D/d
1	0.184	60	0.5	20.1	1.7
2	0.184	60	1.5	38.4	2.2
3	0.184	60	2.5	50.5	2.5
4	0.184	45	0.5	20.1	1.8
5	0.184	45	1.5	38.1	2.0
6	0.184	45	2.5	50.2	2.3
7	0.184	30	0.5	19.9	1.6
8	0.184	30	1.5	38.0	2.0
9	0.184	30	2.5	50.0	2.3
10	0.370	60	0.5	17.1	1.9
11	0.370	60	1.5	32.4	1.9
12	0.370	60	2.5	42.6	2.1
13	0.370	45	0.5	17.0	1.5
14	0.370	45	1.5	32.3	1.8
15	0.370	45	2.5	42.4	2.9
16	0.370	30	0.5	17.0	1.8
17	0.370	30	1.5	32.2	2.0
18	0.370	30	2.5	42.3	2.4

d = nozzle outlet diameter, 12 mm in all cases
D = jet diameter at a distance of 200 mm from nozzle outlet

Tab. II: Calculated pressure losses and impact velocities

Substance	Driving pressure [MPa]	Length of exit pipe [m]	Pressure loss in exit pipe [MPa]	Impact velocity [m/s]
water	2.5	0.184[1)] (0.370)[2)]	0.9 (1.43]	53 (48)
alumina	2.5	0.130[1)] (0.280)[2)]	0.8 (1.25)	35 (30)
iron	2.5	0.270[1)] (0.490)[2)]	1.25 (1.59)	22(17)

[1)] following Latzko,
[2)] following Bowlas/Brighton

Tab. III: Conditions and data of the relevant performance tests

Test No Melt material	Water tests	VJ05 oxide	VJ06 oxide	VJ07 1.iron + 2.oxide	KJ01 1.iron + 2.oxide
Ejected mass (kg)	14	10	10	20 + 20	20 + 20
Nozzle: L/d	15+30	10	10	10	2.1
Temperature (°C)	envir.	2000	2000	(not available)	2050
Max. driving pressure (MPa)	0.5-2.5	0.92	1.5	1.5 1.1	1.5 1.1
Time of ejection (s)	-	-	2.5	2.6 3.4	3.0 >3
Max. jet speed (m/s)	20-50	20.5	25	17 22.3	16.5 21.3
Jet diversion D^*/d	2.3-4.4	2.5	3 - 5.8	2.5 5	1.5 2.5

L = length of nozzle exit pipe
d = nozzle outlet diameter, 12 mm in all cases.
D* = jet diameter at a distance of 300 mm from nozzle outlet
(note: diameter D in Tab. I is related to 200 mm)

Tab. IV: Composition of concrete samples

A. Construction concrete

- Mixture:
  - cement 1.0 kg
  - gravel 5.5 kg
  - water 0.39 liters (6 wt-%)

- Cement:
  Portland CEM I 32.5 R
  ($\geq 32.5 \geq 52.5$ N/mm^2)

- Gravel:
  Type 'Rheinkies'

Grain size		
	0/2 mm	37 %
	2/8mm	20 %
	8/16 mm	23 %
	16/32 mm	20 %

- Sample size 320 mm x 200 mm x 100 mm

- Amounts to fabricate two samples:
  about 5 kg cement, 27 kg gravel, 1.95 l water

B. Borosilicate glass concrete

- Mixture:
  - cement 18.3 %
  - glass 70.92 %
  - water+solvent 10.98 %

- Cement:
  Portland CEM I 32.5 R

- Borosilicate glass:

Grain size		
	0-1 mm	50 %
	1-2mm	15 %
	2-4 mm	15 %
	4-8 mm	20 %

- Water + solvent:
  Water-cement-value 0.6
  Solvent dose 30 ml/kg cement
  Solvent type FM-F, Heidelberger Zementwerke

- Sample size 320 mm x 200 mm x 100 mm

- Amounts to fabricate two samples:
  about 5.8 kg cement, 22.5 kg glass, 0.19 kg solvent, 3.3 l water

Tab. V: Conditions and results of the KJ02, KJ03, KJ04 and KJ08 tests with siliceous concrete (construction concrete)

Test No. **Melt material**	**KJ02** **iron/oxide**	**KJ03** **iron/oxide**	**KJ04** **only oxide**	**KJ08** **iron/oxide**
Ejected mass, kg	18.8 / 21.2	52.7 / 59.3	83	75 / 84.5
Duration of impact , according to post-calculation s	3.6 / 6.3	6 / 7	10	5.8 / 2.9
Temperature of melt jet, °C	2100	1850	2050	2050
Max. driving pressure (av. pressure), MPa	0.3	0.5	0.5 (∅ 0.43)	0.8
Speed of melt jet (calculated), m/s	7.7 / 11.5	8.8 / 14.1	14.1	12.1 / 17.8
Horiz. extension of erosion, mm	65x50 / 55x70	90 x 90	∅ 90-120	∅ 60/∅ 70
Erosion depth, mm	25 / 15	85	60	65 / 29
Eroded volume, ml	45 / 40	350	360	180 / 95
Average vertical erosion rate (calc.), mm/s	8.9 / 4.5	8.3	≈ 4.8	11.2 / 10
Average volume erosion rate, ml/s	-	-	36	31 / 33
Radial erosion of nozzle, (from 12 mm) mm	22	24	20-24	25

In KJ03, the revolving mechanism failed. Only one concrete sample was eroded.

Tab. VI: Conditions and results of the KJ05, KJ06 and KJ07 tests with borosilicate glass concrete

Test No. **Melt material**	**KJ05** **iron / oxide**	**KJ06** **iron / oxide**	**KJ07** **iron / oxide**
Ejected mass, kg	49 / 55	54 / 61	71.5 / 80.5
Duration of impact , according to post-calculation s	6.1 / 5.7	7.3 / 4.6	6.3 / 3.9
Temperature of melt jet, °C	2150	2100	2100
Max. driving pressure (av. pressure), MPa	0.5 (∅ 0.49)	0.4 (av. 0.36)	0.8
Speed of melt jet (calculated), m/s	9.9 / 14.4	8.5 / 12.5	12.4 / 18.0
Horiz. extension of erosion, mm	∅ 60 / 150	75 x 65 / ∅ 90	50 x 60 / ∅ 90
Erosion depth, mm	33 / 23	38 / 13	45 / 20
Eroded volume, ml	39 / 120	92 / 59	95 / 110
Average vertical erosion rate (calc.), mm/s	6.7 / 4.0	5.2 / 2.8	8 / 5.1
Average volume erosion rate, ml/s	8.0 / 21.0	12.6 / 12.8	15.1 / 28.2
Radial erosion of nozzle, from 12 mm) mm	25-26	27-28	28-29

Tab. VII: Summary table, vertical erosion rates (from Tab. V and VI)

Vertical erosion rate, siliceous concrete			
Experiment	KJ02	KJ04	KJ08
Driving pressure, MPa	0.3	0.5	0.8
Iron, rate, mm/s	8.9	-	11.2
Oxide, rate, mm/s	4.5	4.8	10.0
Vertical erosion rate, borosilicate glass concrete			
Experiment	KJ06	KJ05	KJ07
Driving pressure, MPa	0.4	0.5	0.8
Iron, rate, mm/s	5.2	6.7	8.0
Oxide, rate, mm/s	2.8	4.0	5.1

10 Figures

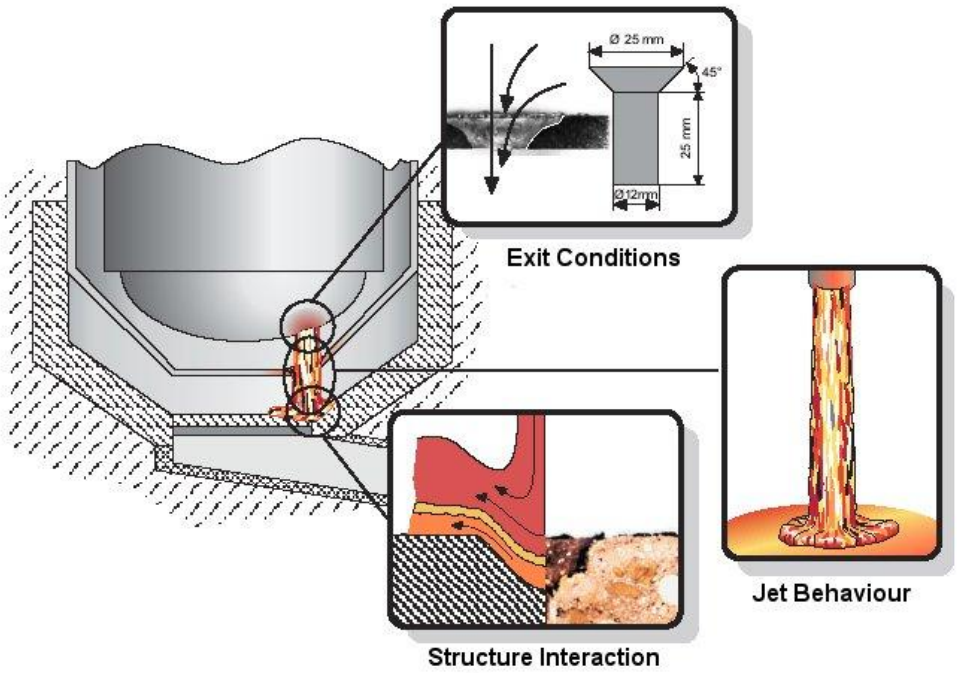

Fig. 1.1: Sketch of scenario (prepared by RUB, see refs. 9, 10)

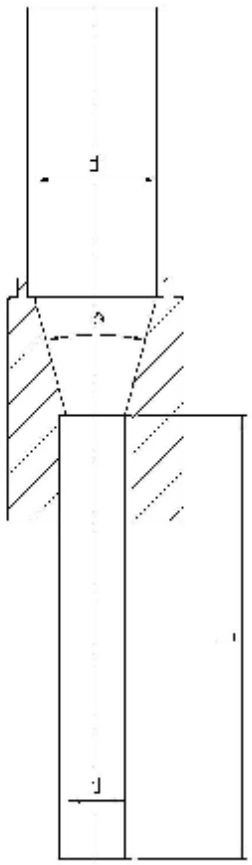

Fig. 2.1: Water experiments, nozzle design

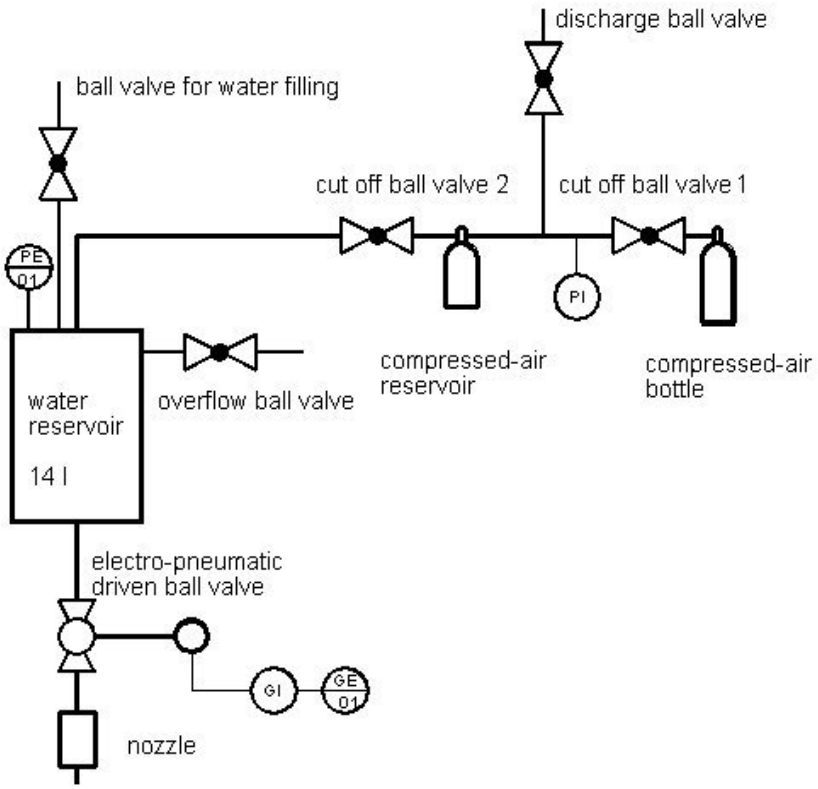

Fig. 2.2: Water experiments, experimental setup

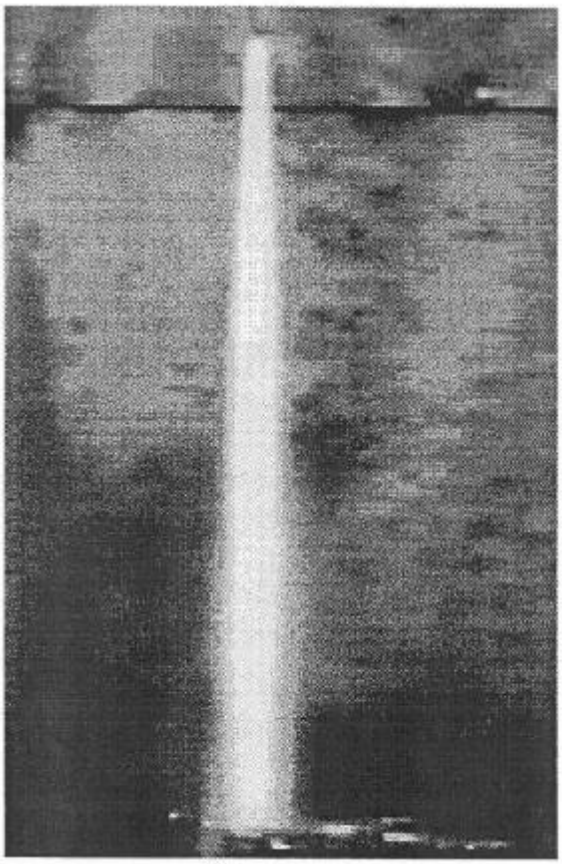

Fig. 2.3: AV61, α= 30 °, Δp = 25 bar, l = 0.370 m

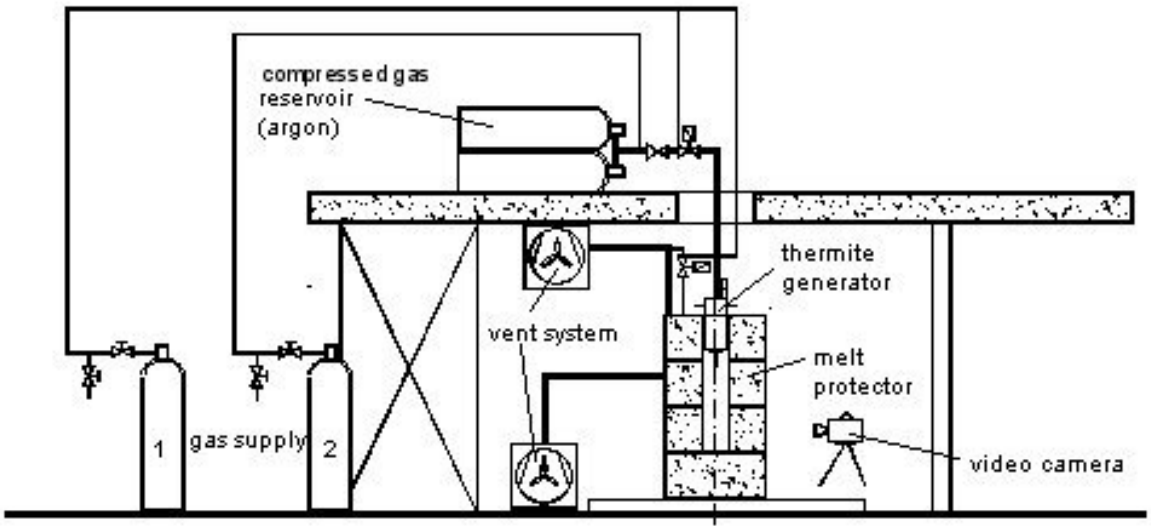

Fig. 3.1: Thermite performance tests, experimental setup

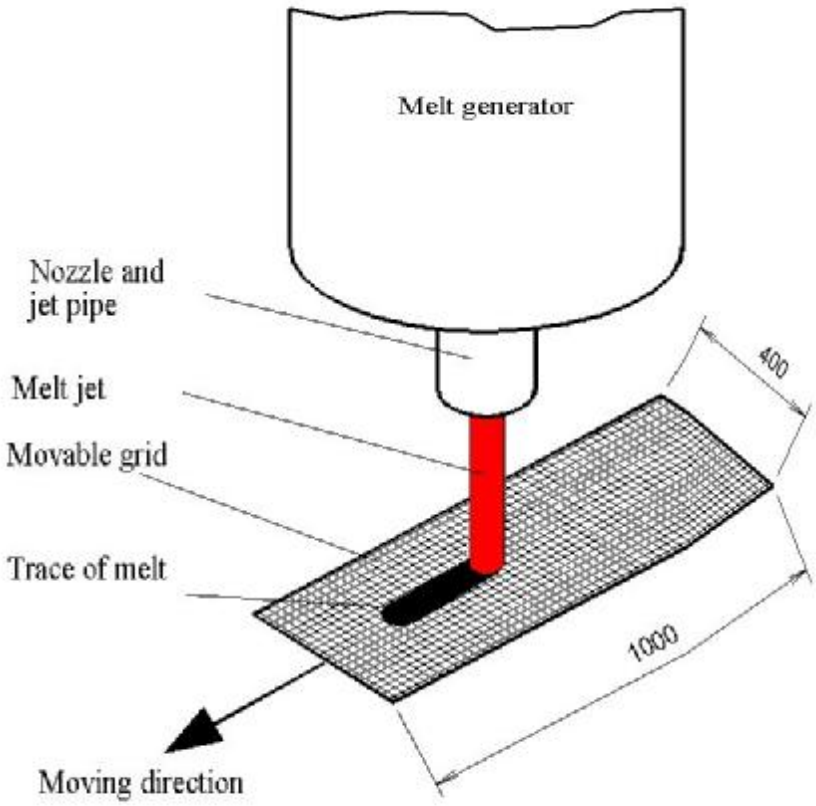

Fig. 3.2: Thermite performance tests, detail of the experimental facility, schematically

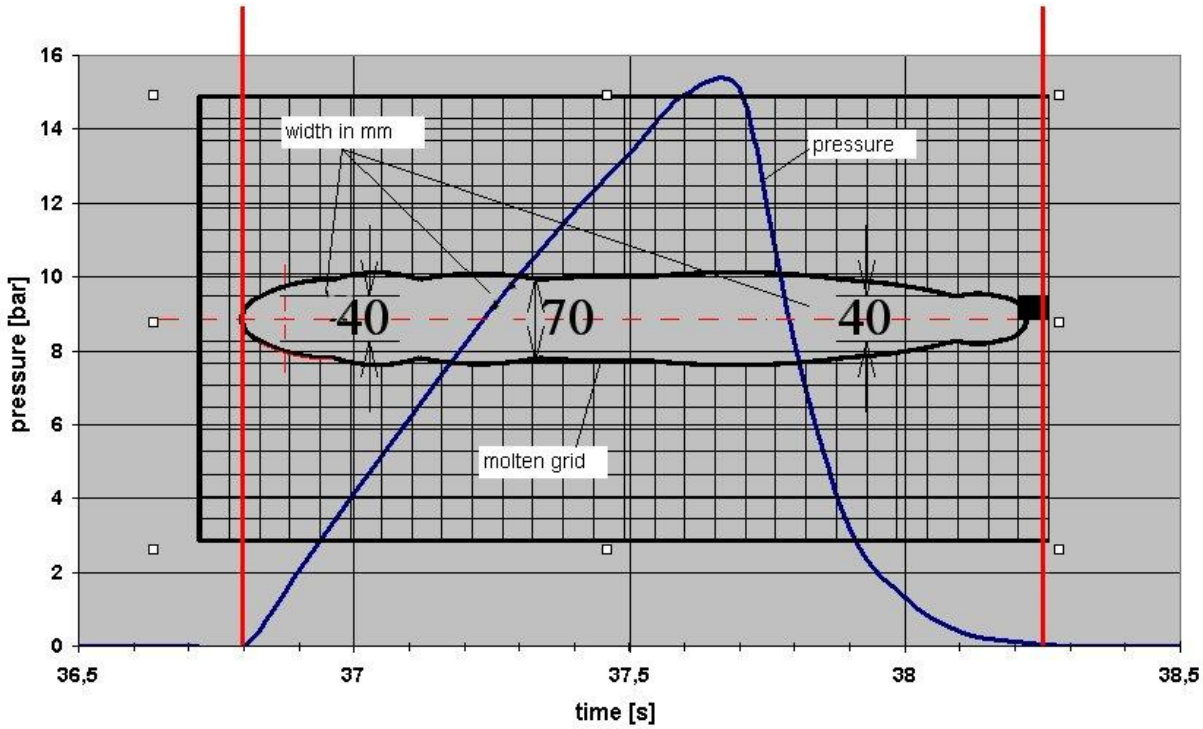

Fig. 3.3: Thermite performance tests, footprint in the grid, correlated to the pressure-time history

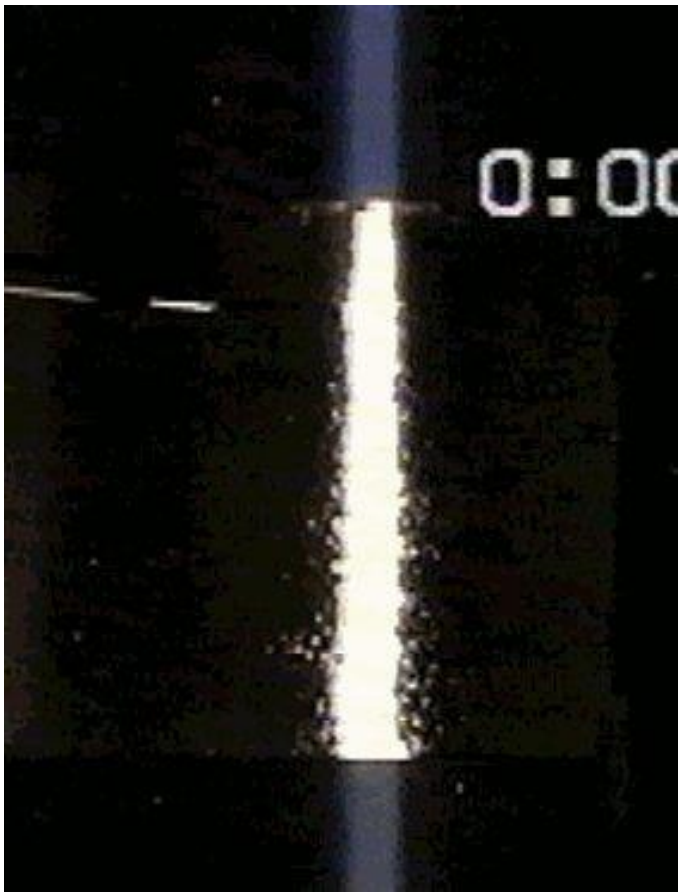

Fig. 3.4: Thermite performance tests, oxide jet, experiment VJ06

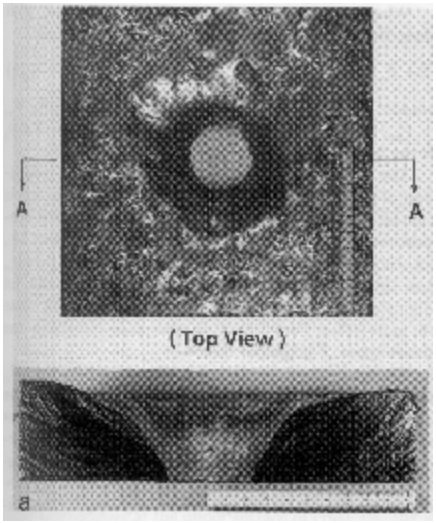

(a) PNC experiments with salt melts and tin plates

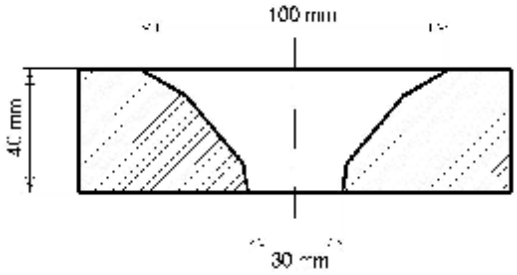

(b) KTH experiments with oxide melts and lead plates

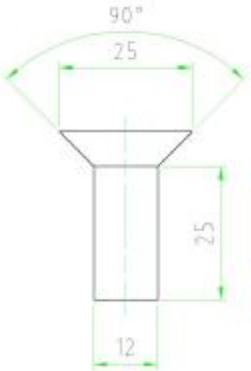

(c) KAJET experiments, geometry of the nozzle

Fig. 3.5: Results of wall erosion tests performed with various simulant materials at PNC and KTH compared with the nozzle geometry used in the KAJET erosion experiments

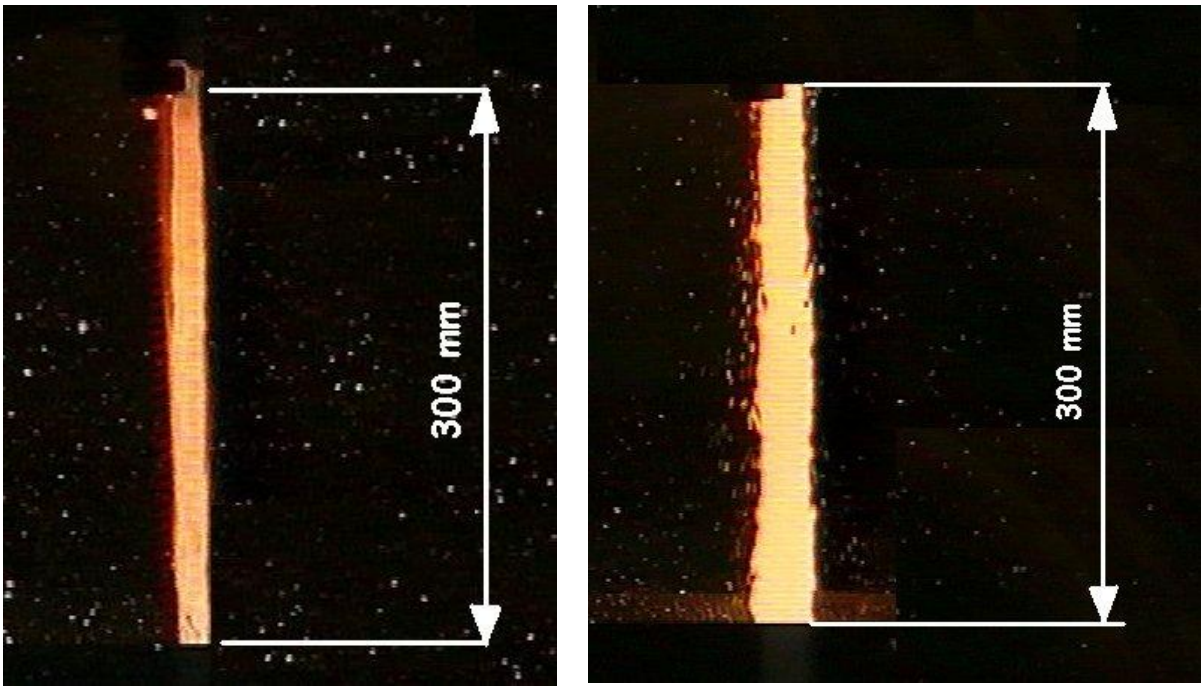

(a) iron jet (b) alumina jet

Fig. 3.6: Also with a short exit pipe (25 mm) and a bigger angle of the nozzle (90°), a sufficiently compact jet is achieved for both metallic and oxidic melt

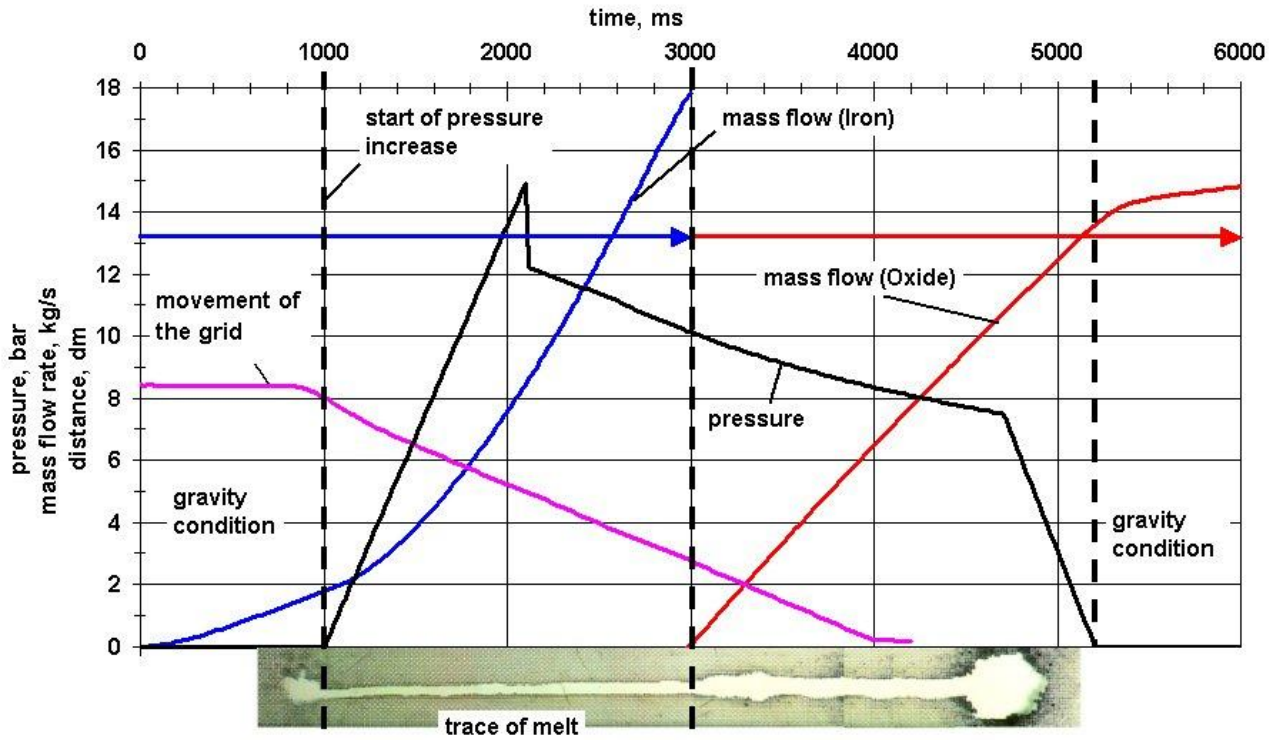

Fig. 3.7: Experiment KJ01, various data showing the course of events

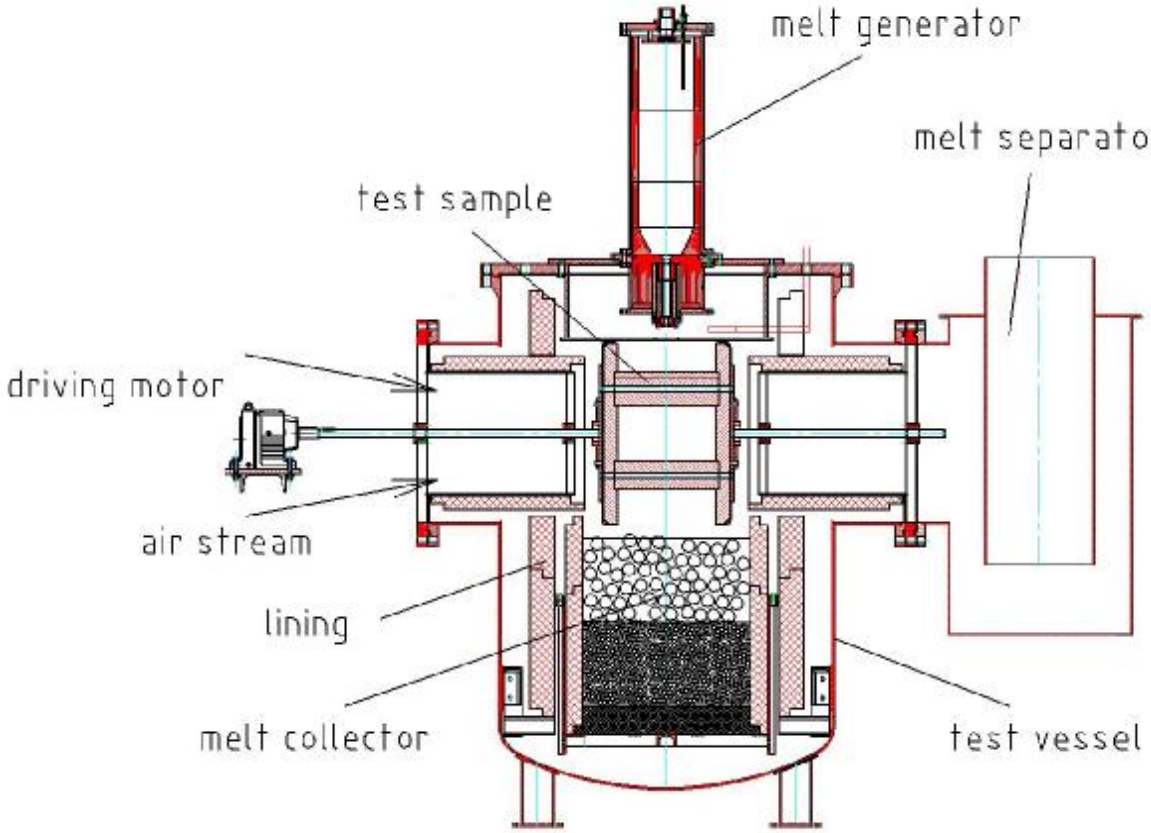

Fig. 4.1: Erosion test facility

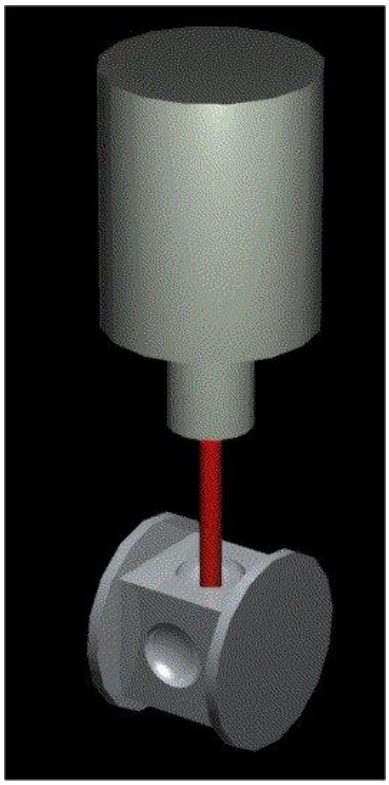

Fig. 4.2: Arrangement of melt source, jet, and plate carrier with two concrete samples

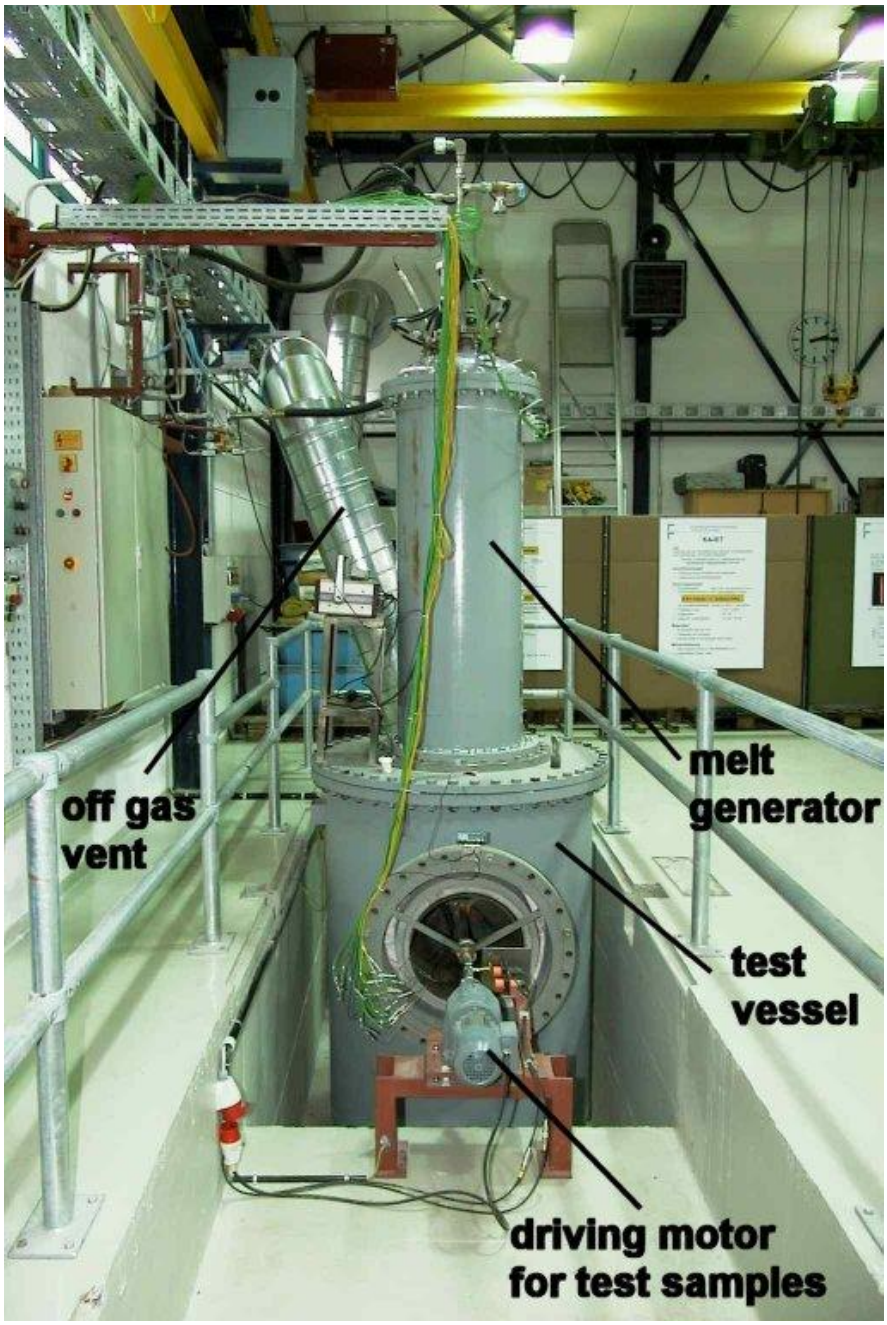

Fig. 4.3: Experimental facility

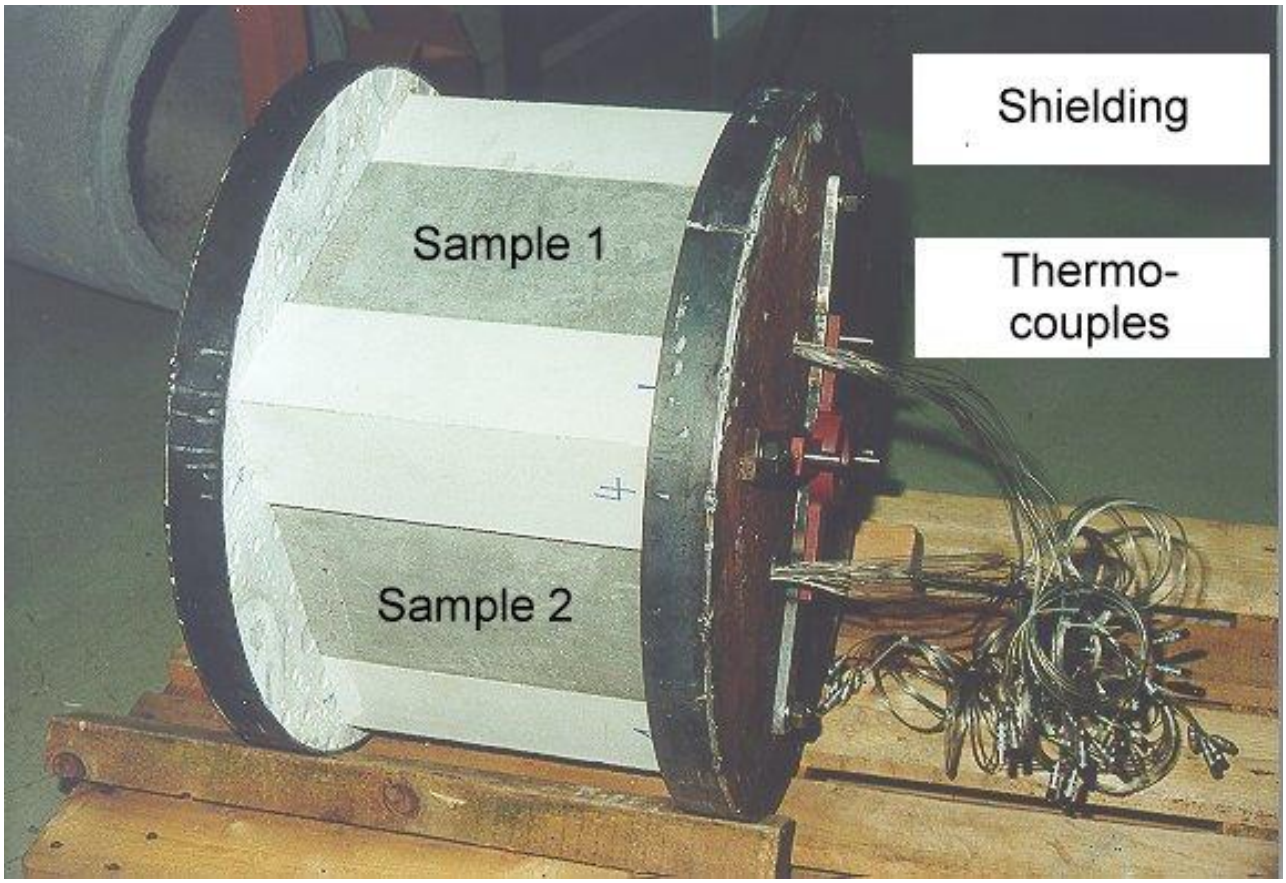

Fig. 4.4: Revolving sample carrier

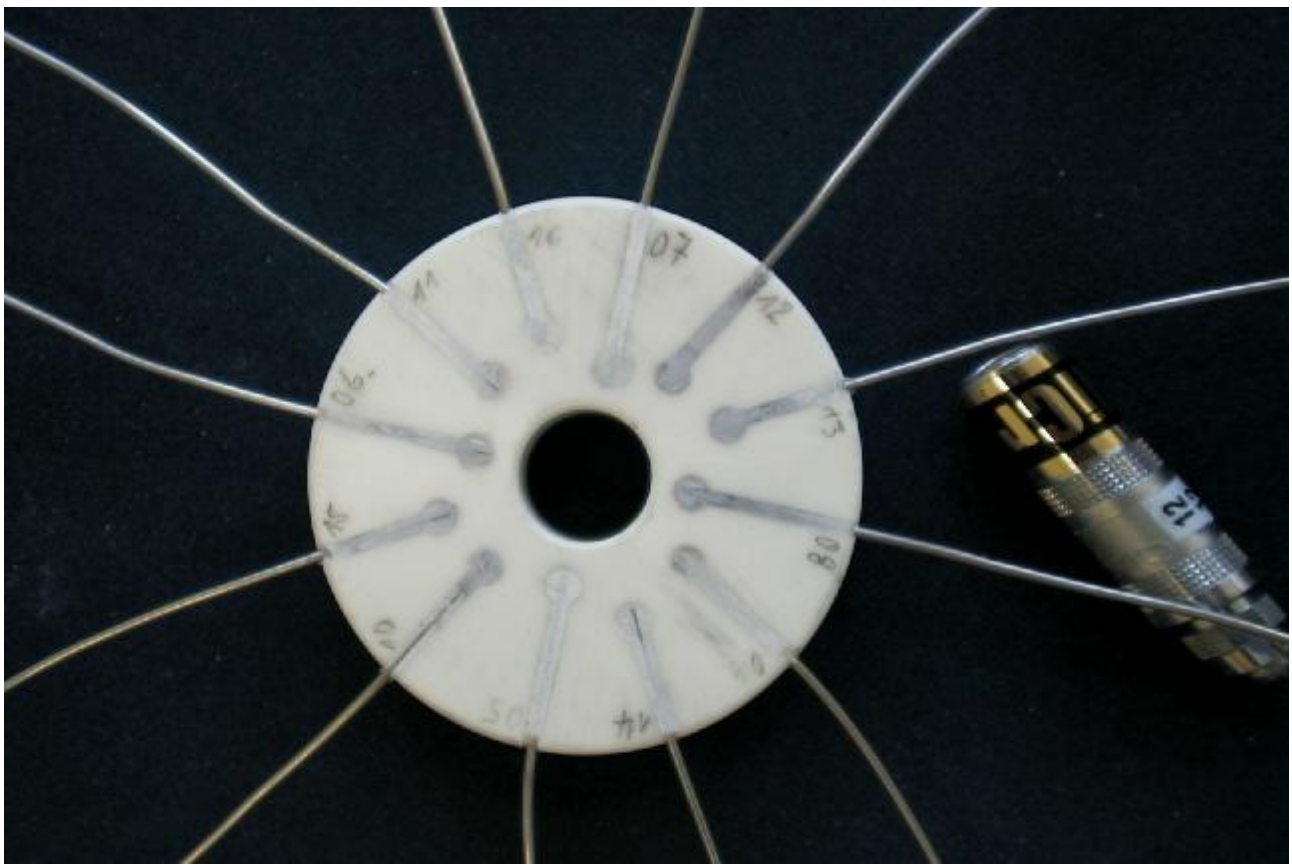

Fig. 4.5: Instrumented nozzle

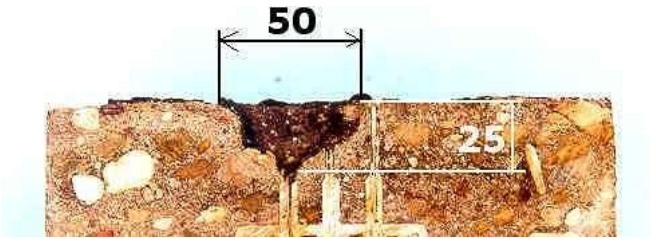

(a) Concrete sample eroded by Fe melt

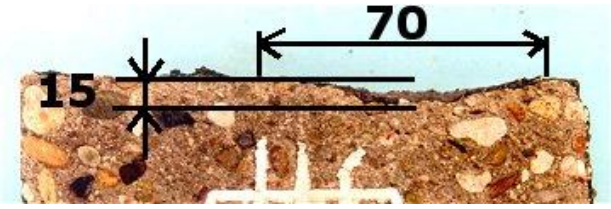

(b) Concrete sample eroded by Al_2O_3 melt

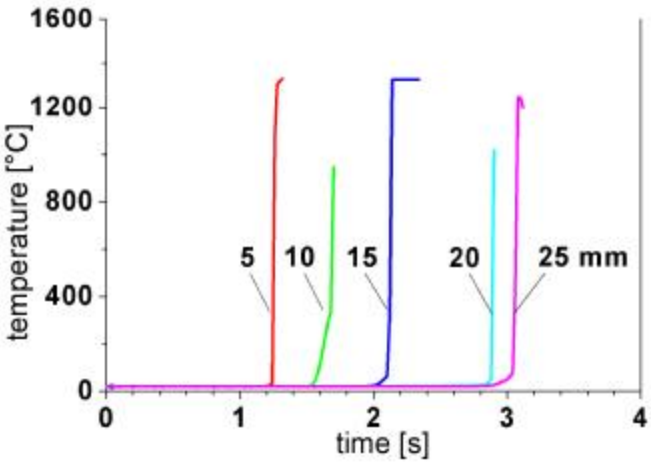

(c) Temperature rise and failure of the thermocouples

KJ02, erosion by Al_2O_3 melt, no signals available

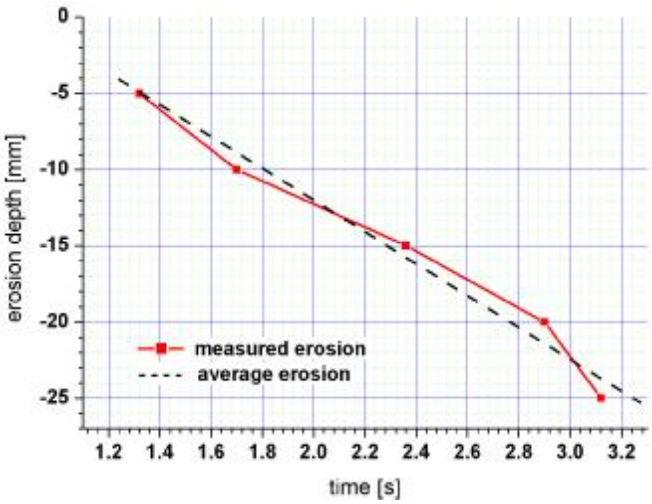

(d) Average erosion rate by Fe melt = 8.9 mm/s

KJ02, erosion by Al_2O_3 melt, no signals available

Fig. 4.6: KJ02, eroded siliceous concrete samples

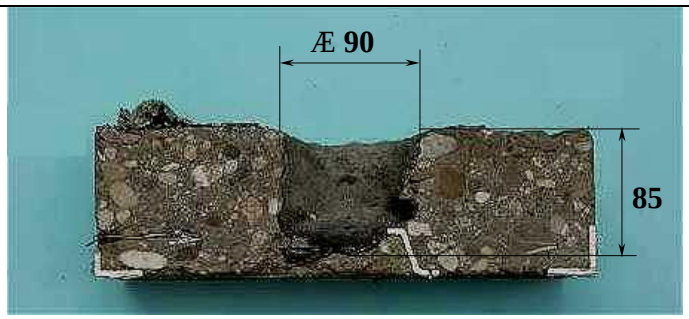

(a) Concrete sample eroded by Fe melt

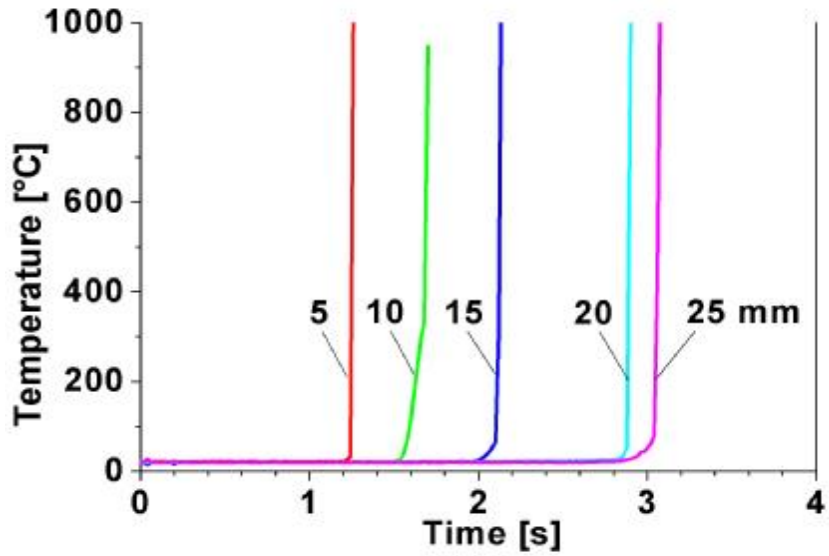

(b) Temperature rise and failure of the thermocouples

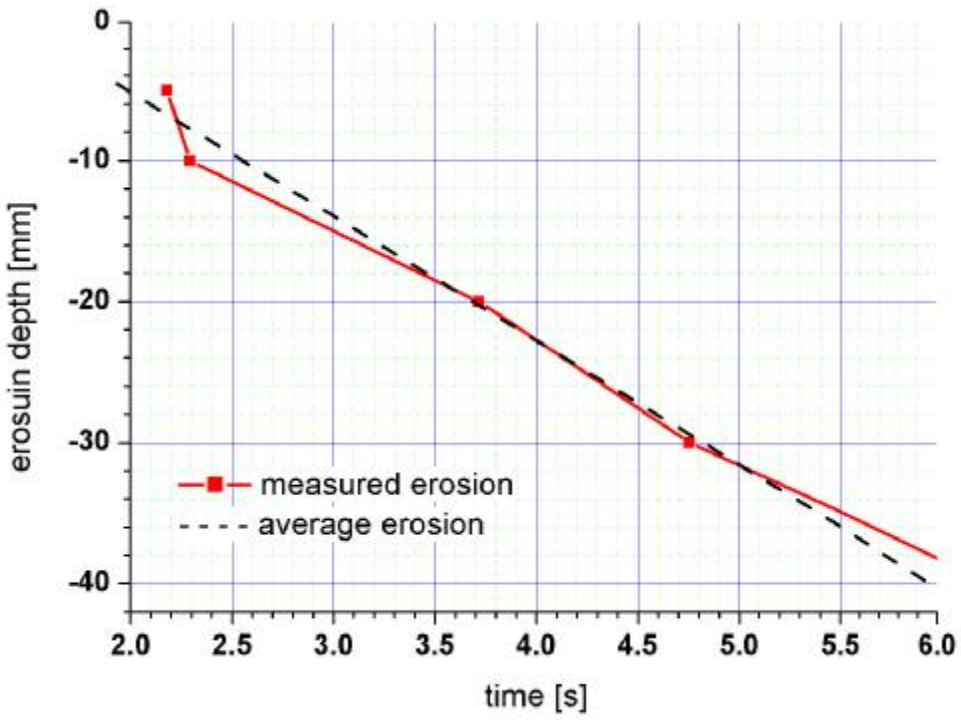

(c) Average erosion rate by Fe melt = 7.7 mm/s

Fig. 4.7: KJ03, eroded siliceous concrete samples. Revolving sample carrier failed, the melt was ejected only on the Fe sample

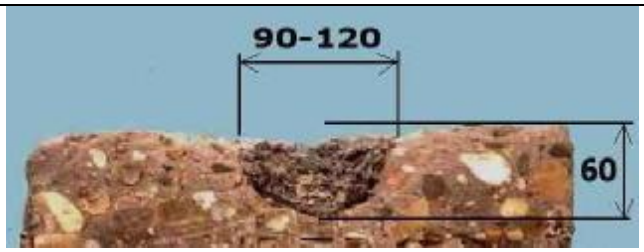

(a) Concrete sample eroded only by Al_2O_3 melt

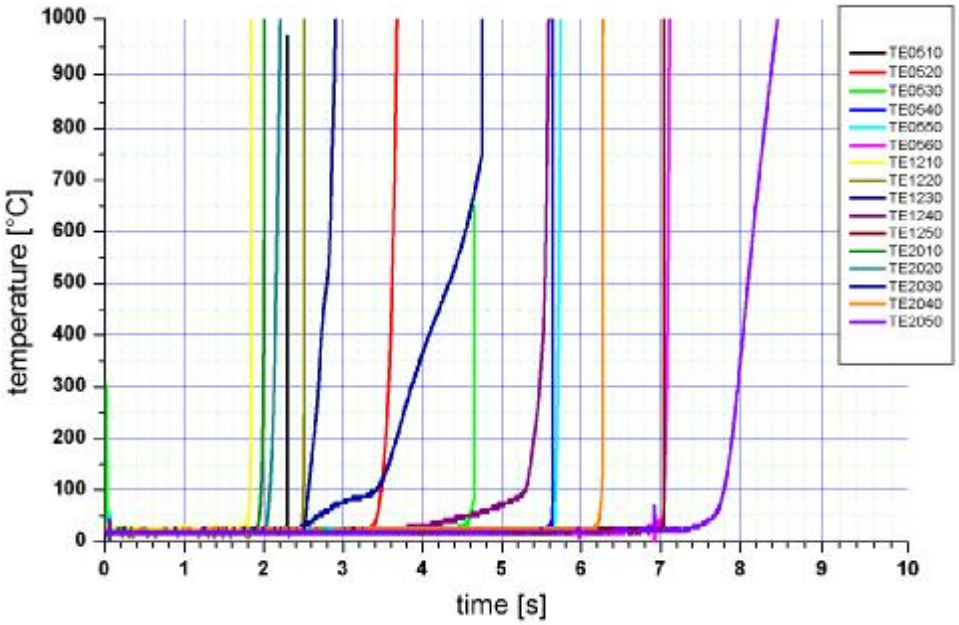

(b) Temperature rise and failure of the thermocouples

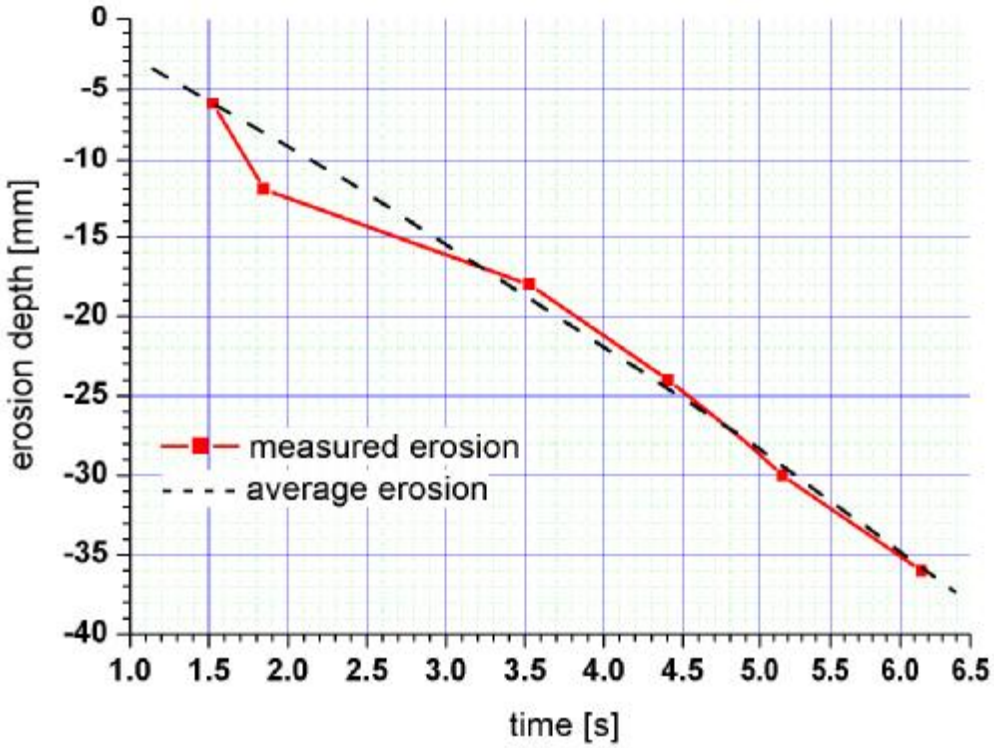

(c) Average erosion rate by Al_2O_3 melt = 4.8 mm/s

Fig. 4.8: KJ04, eroded siliceous concrete samples

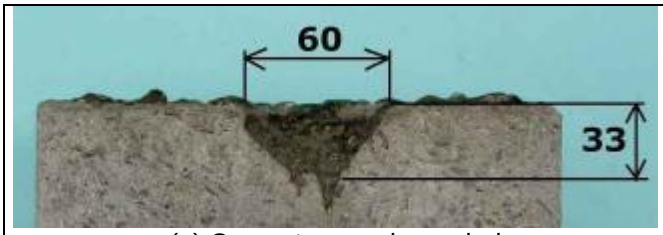

(a) Concrete sample eroded by Fe melt

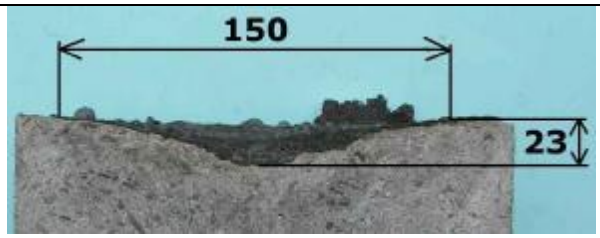

(b) Concrete sample eroded by Al_2O_3 melt

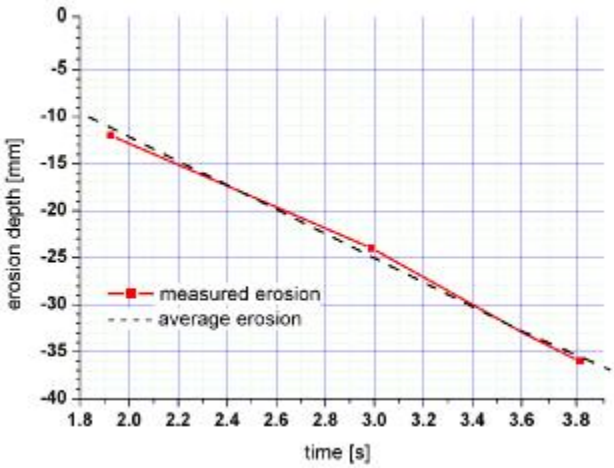

(c) Average erosion rate by Fe melt = 6.5 mm/s

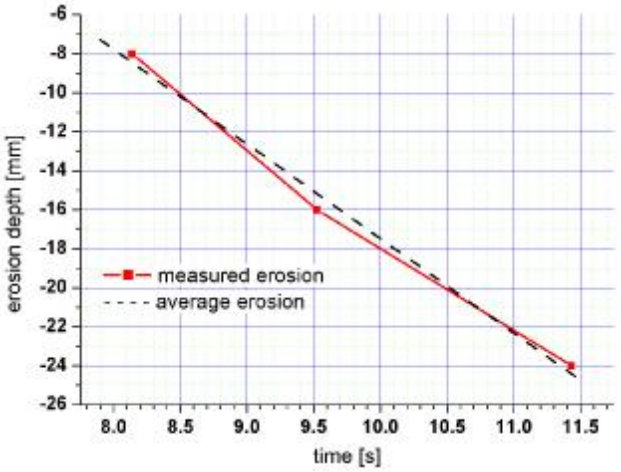

(d) Average erosion rate by Al2O3 melt = 3.8 mm/s

Fig. 4.9: KJ05, eroded borosilicate glass concrete samples

(a) Concrete Sample eroded by Fe melt

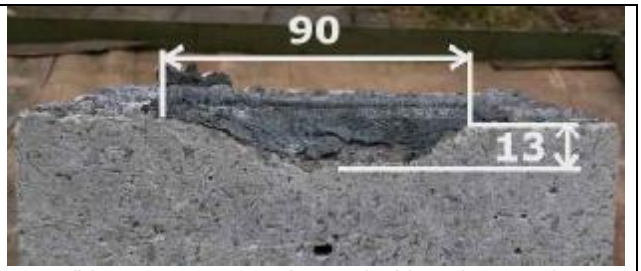

(b) Concrete sample eroded by Al_2O_3 melt

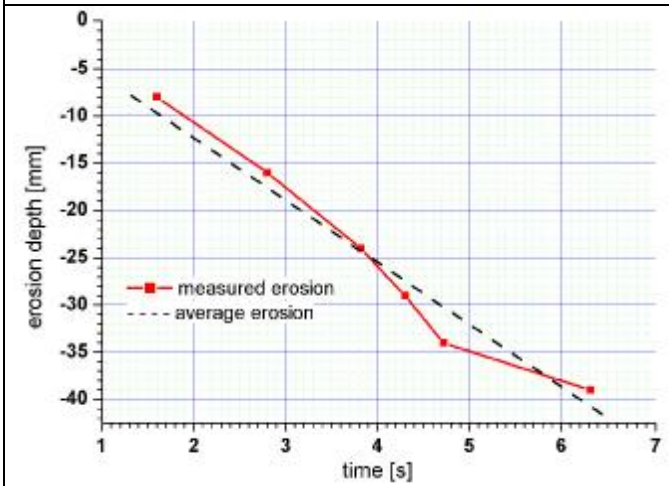

(c) Average erosion rate by Fe melt = 5.2 mm/s

KJ06, thermocouples destroyed, signals not available

Fig. 4.10: KJ06, eroded borosilicate glass concrete samples

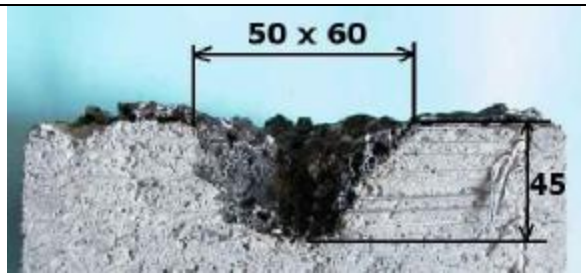

(a) concrete sample eroded by Fe melt

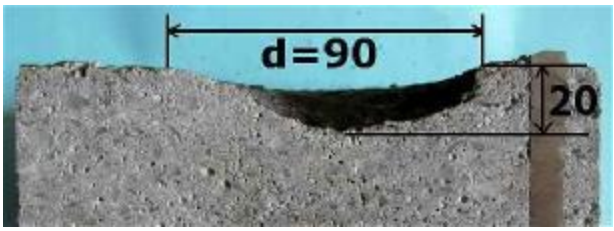

(b) Concrete sample eroded by Al_2O_3 melt

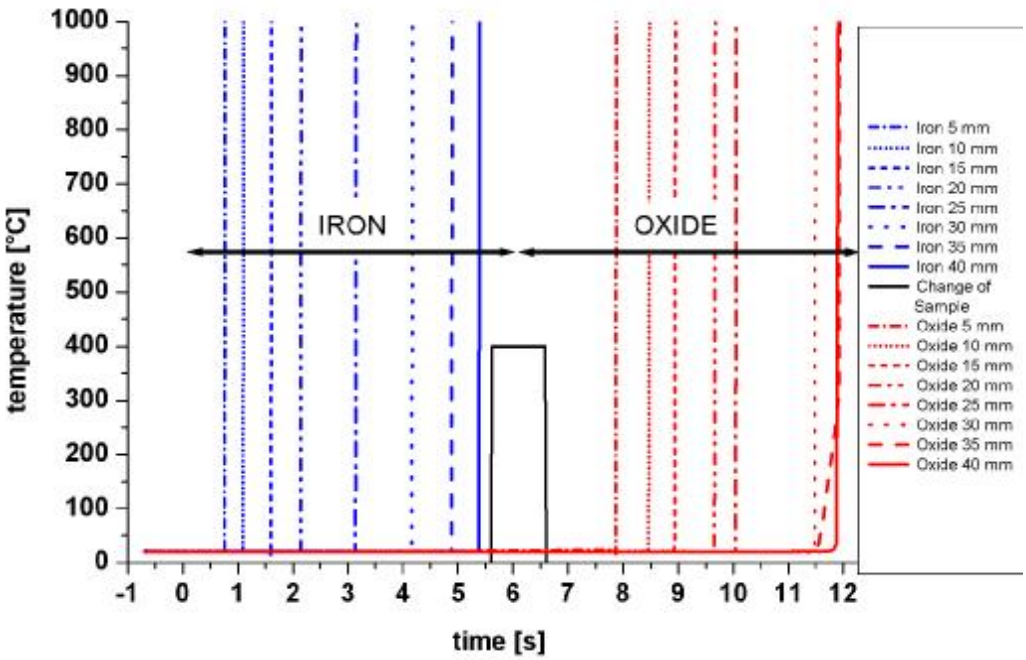

(c) Temperature rise and failure of the thermocouples

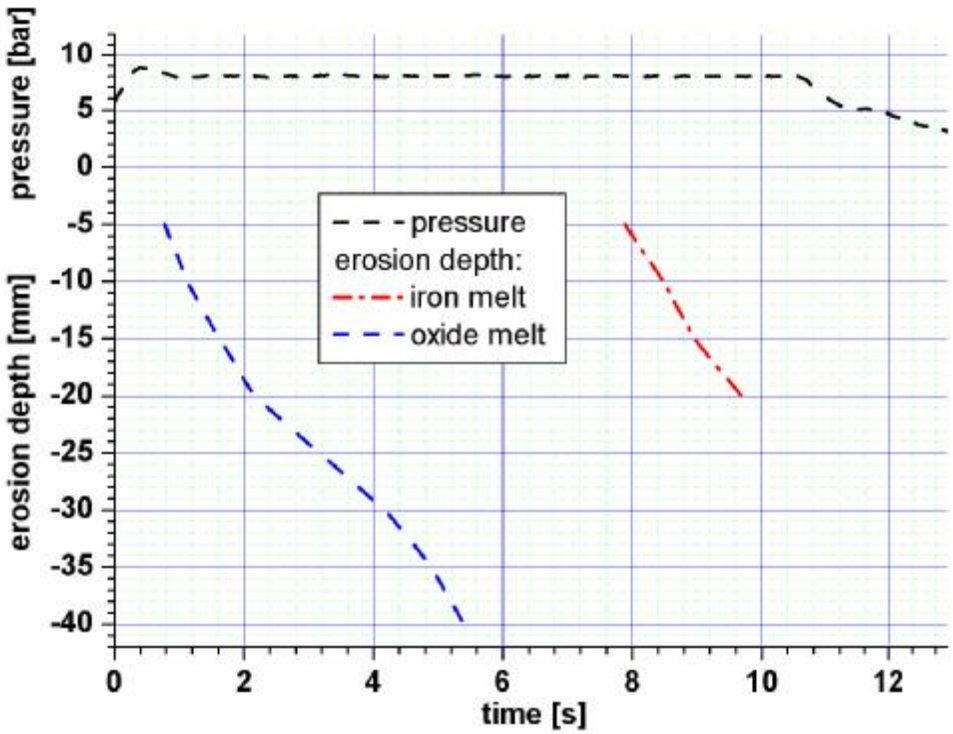

(d) Average erosion rates: Fe melt = 8.0 mm/s, Al_2O_3 melt = 5.1 mm/s

Fig. 4.11: KJ07, eroded borosilicate glass concrete samples

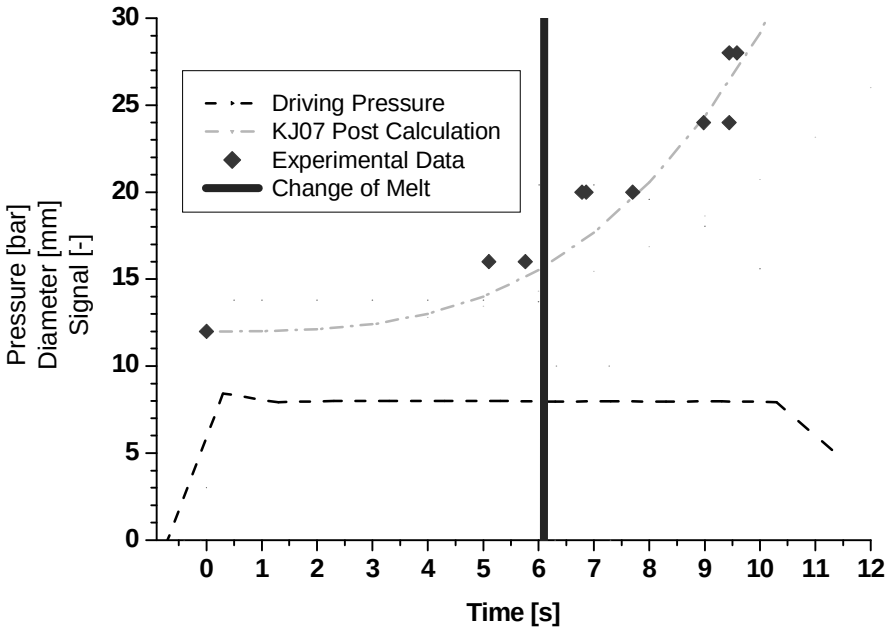

Fig. 4.12 Experimental data and post calculation of the nozzle erosion over time during test KJ07

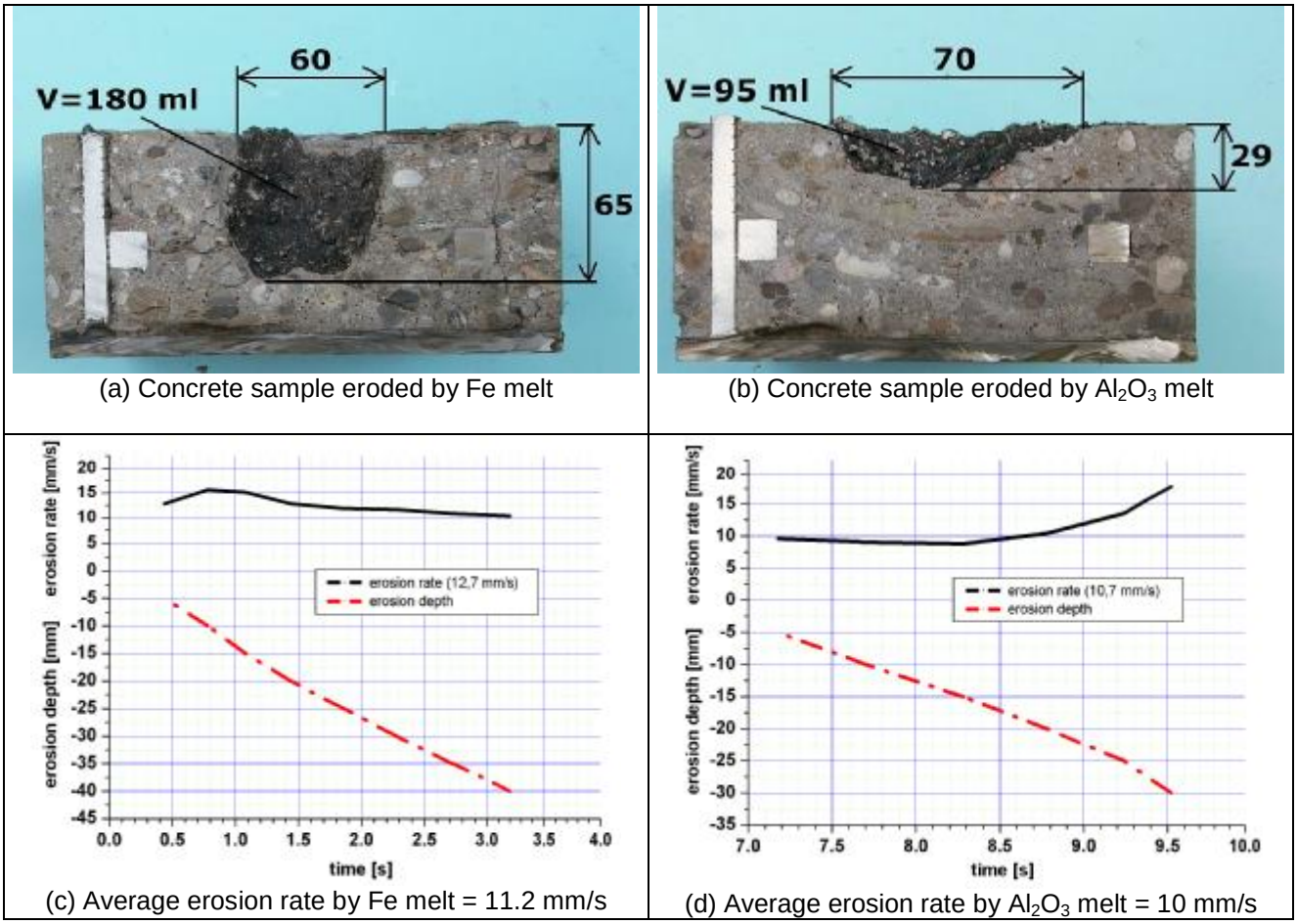

(a) Concrete sample eroded by Fe melt

(b) Concrete sample eroded by Al_2O_3 melt

(c) Average erosion rate by Fe melt = 11.2 mm/s

(d) Average erosion rate by Al_2O_3 melt = 10 mm/s

Fig. 4.13: KJ08, eroded siliceous concrete samples